Upcycling Municipal Solid Waste to Polymers and Bioethanol

Euncheol Ra[a], Yoel Cortés-Peña[a], David Rivera-Kohr[b], Lily Callen[a], Panzheng Zhou[a], Jiuling Yu[a], Charles Granger[a], Nepu Saha[c], Jordan Klinger[c], John Estela-García[d], Fei Long[e], Trey K. Sato[f], Morgan Davies[f], Harrison Appiah[g], Kevin Nelson[h], Kevin Guigley[h], Bumjun Kwon[a], Kyuhyeok Choi[a], Priscilla Lee[a], Lewis Tanner[b], Brittney Vo[b], Armando G. McDonald[g], Tim Osswald[d], Victor Zavala[a], Reid C. Van Lehn[a,f], Ezra Bar-Ziv[e], Brian Fox[b], George W. Huber[a,*]

[a] Department of Chemical & Biological Engineering, University of Wisconsin-Madison, Madison, WI 53706, USA

[b] Department of Biochemistry, University of Wisconsin-Madison, Madison, WI 53706, USA

[c] Energy and Environment Science & Technology Directorate, Idaho National Laboratory, Idaho Falls, ID 83415, USA

[d] Department of Mechanical Engineering, University of Wisconsin-Madison, Madison, WI 53706, USA

[e] Department of Aerospace and Mechanical Engineering, Michigan Technological University, Houghton, MI 49931, USA

[f] DOE Great Lakes Bioenergy Research Center, University of Wisconsin-Madison, Madison, WI 53726, USA

[g] Department of Forest, Rangeland and Fire Sciences, University of Idaho, Moscow, ID 83844, USA

[h] Amcor, Neenah Innovation Center, Neenah, WI 54956, USA

** Corresponding author*

Email address: gwhuber@wisc.edu (George W. Huber)

This supplementary material contains:

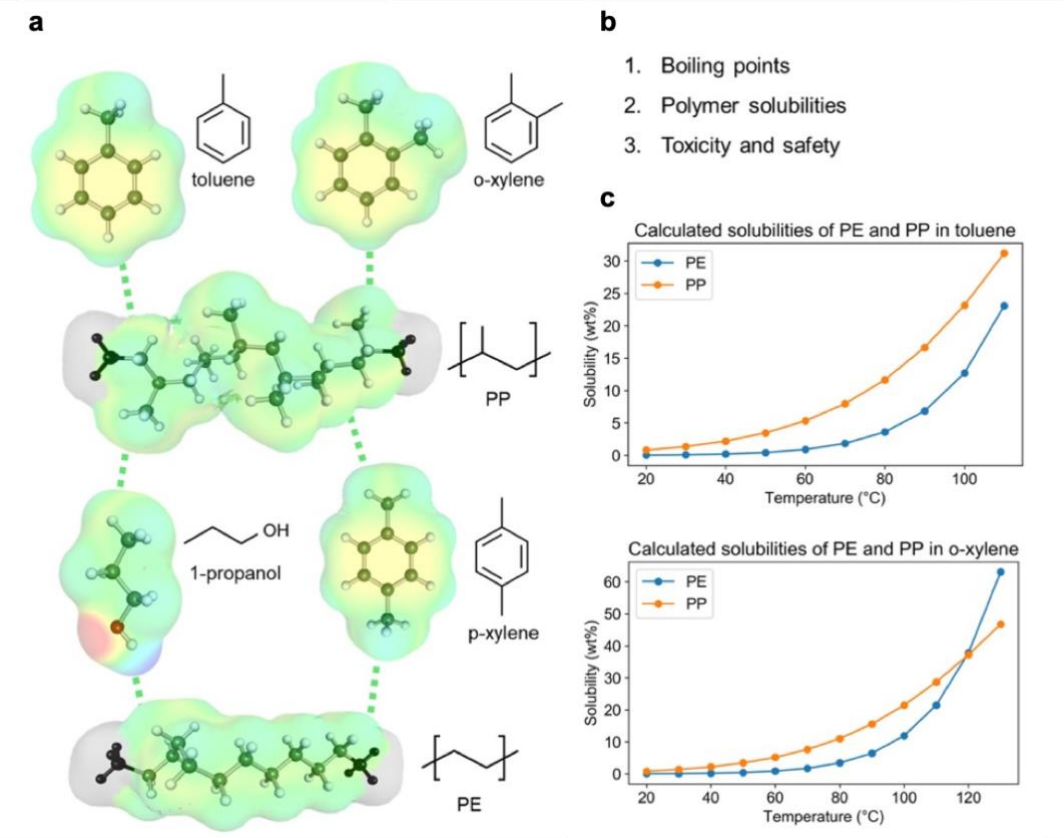

Supplementary Fig. 1. Examples of computational models and solubility calculation results.
a, Screening charge distributions (colored surfaces) are calculated based on molecular structures of polymers and solvents. Oligomer molecules with end groups neglected (gray surface) are used to represent the chemical properties of longer polymer chains. The intermolecular interactions between polymers and solvents are quantified using the COSMO-RS approach based upon the screening charge distributions (dashed lines). **b,** Solvents are selected based on considerations of several properties. **c,** Solubility calculation results for PE and PP in toluene and xylene.

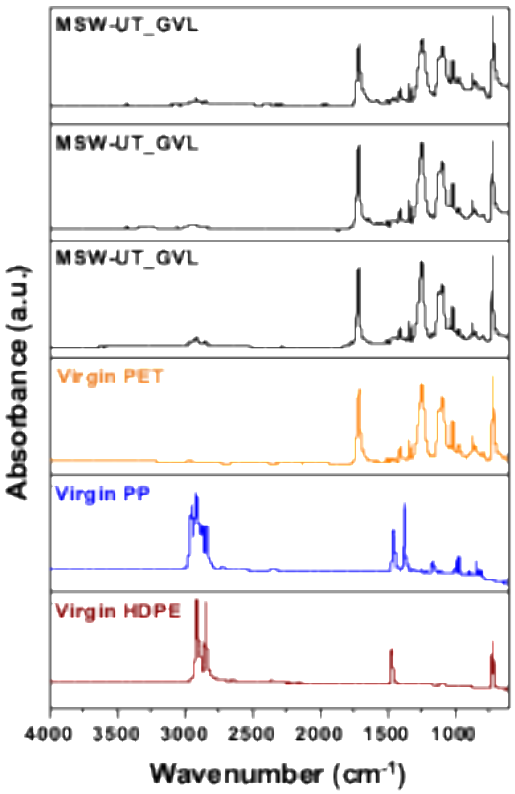

Supplementary Fig. 2. FT-IR spectra of virgin polymers and recovered PET from the second STRAP stage, which uses GVL to process the residues from the first STRAP stage with xylene.

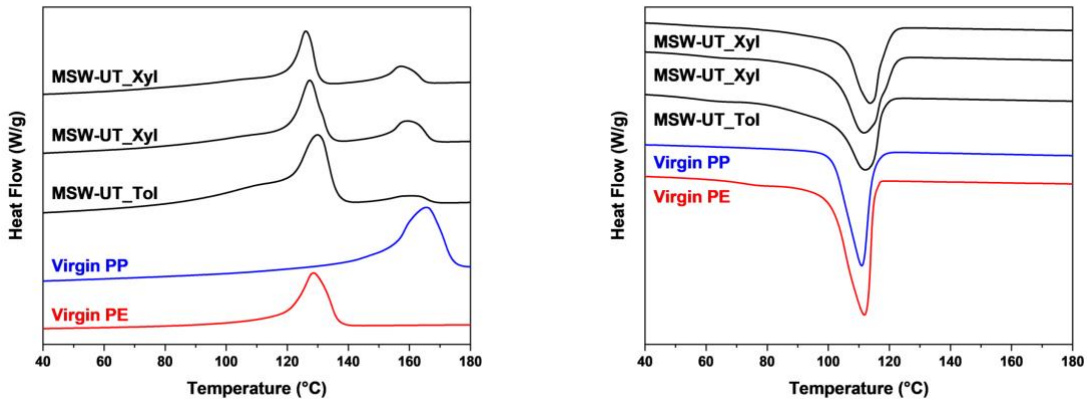

Supplementary Fig. 3. DSC of virgin polymers and recovered polyolefins from the first STRAP stage with toluene and xylene.

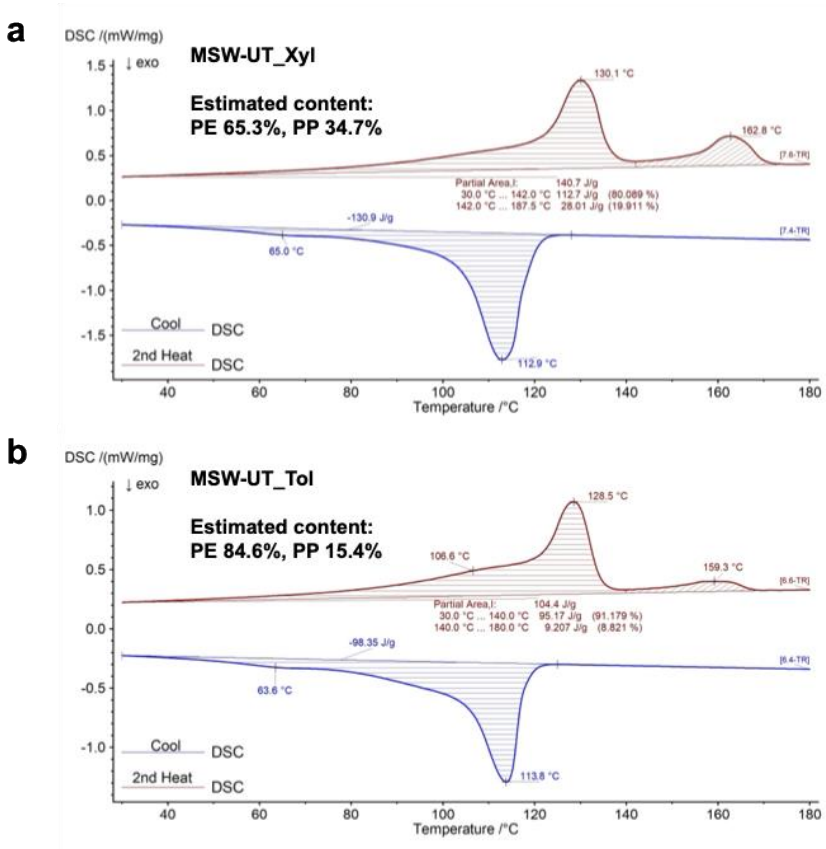

Supplementary Fig. 4. DSC of recovered polyolefins.
a, STRAP-MSW-UT with xylene. **b,** STRAP-MSW-UT with toluene. By taking into consideration the enthalpy of fusion of the total sample and performing a partial peak analysis, the percentage of PE and PP are estimated as 65.3% and 34.7%, respectively, for the recovered polyolefins from STRAP with xylene. For the recovered polymer with toluene, the percentage of PE and PP are estimated to be 84.6% and 15.4%, respectively.

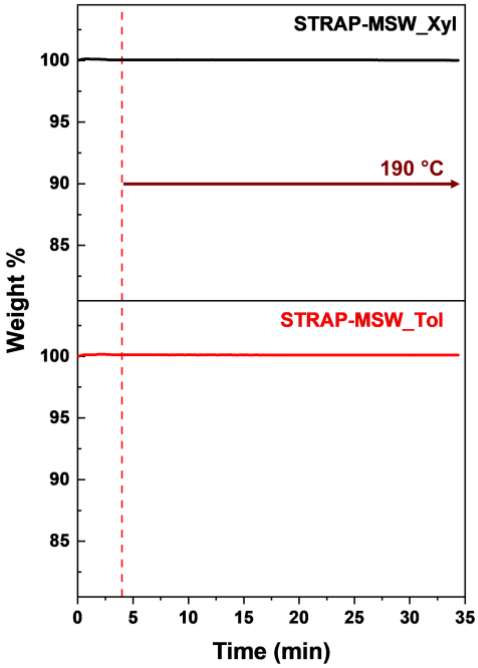

Supplementary Fig. 5. TGA isotherm at 190 °C with the recovered polyolefins from STRAP MSW-UT.

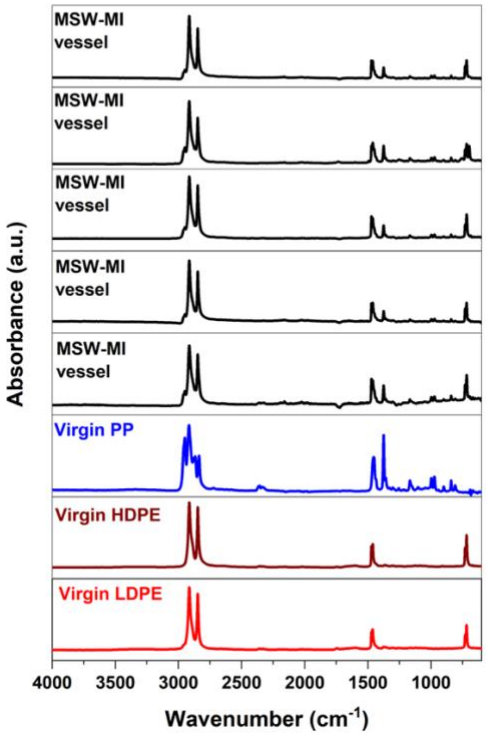

Supplementary Fig. 6. FT-IR spectra of virgin polymers and the recovered polyolefins obtained from MSW-MI using the STRAP process in a jacketed vessel.

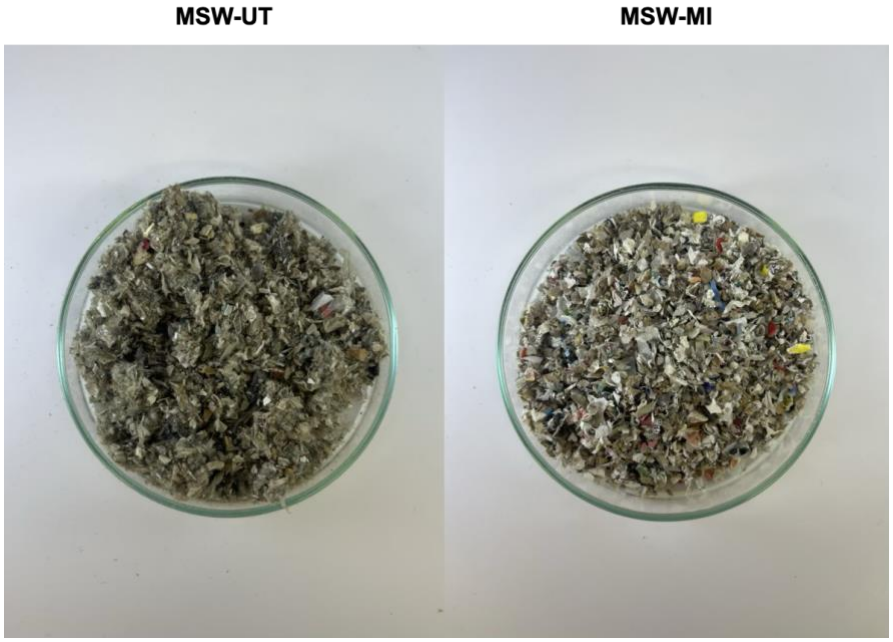

Supplementary Fig. 7. Images of MSW-UT and MSW-MI used for the STRAP experiments (MSW-UT and MSW-MI after identical pre-processing). Despite undergoing the same treatment, the two feedstocks exhibit pronounced heterogeneity in composition, reflecting the intrinsic variability of MSW streams.

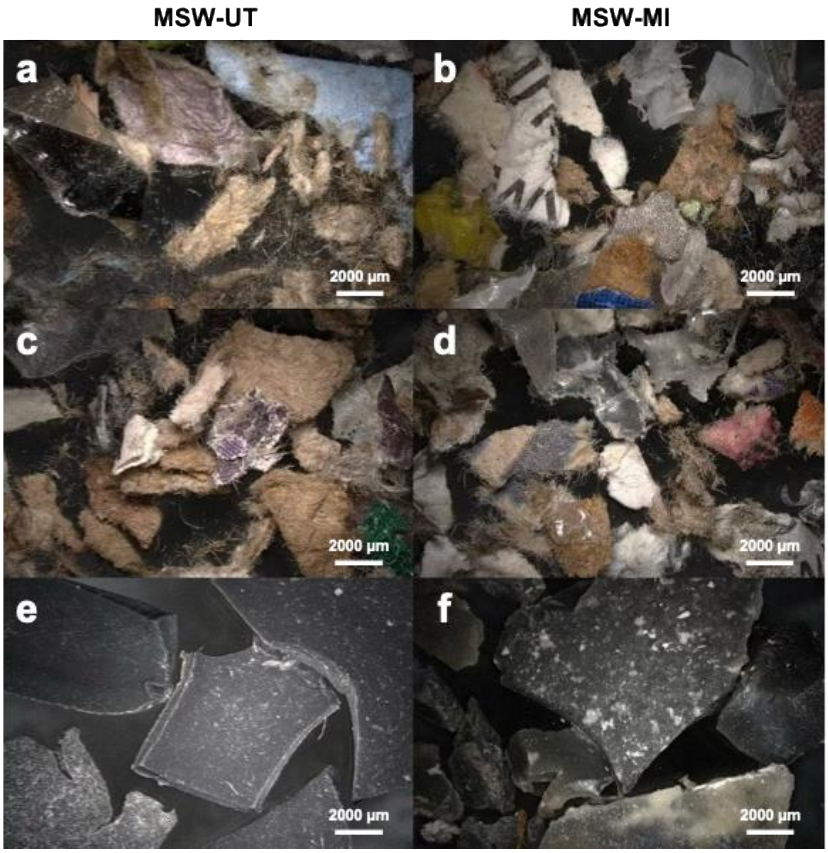

Supplementary Fig. 8. Optical microscope images of raw MSW-UT and MSW-MI (**a-b**), biogenic residues obtained after the STRAP process (**c-d**), and recovered polymers via xylene-based STRAP processing for MSW-UT and MSW-MI (**e-f**), respectively. Raw MSW samples exhibit high heterogeneity, containing plastics, fibrous paper, and other materials. Biogenic residues are dominated by fibrous matter but also contain traces of residual plastics. In contrast, recovered polymers show more uniform textures and surfaces across both feedstocks.

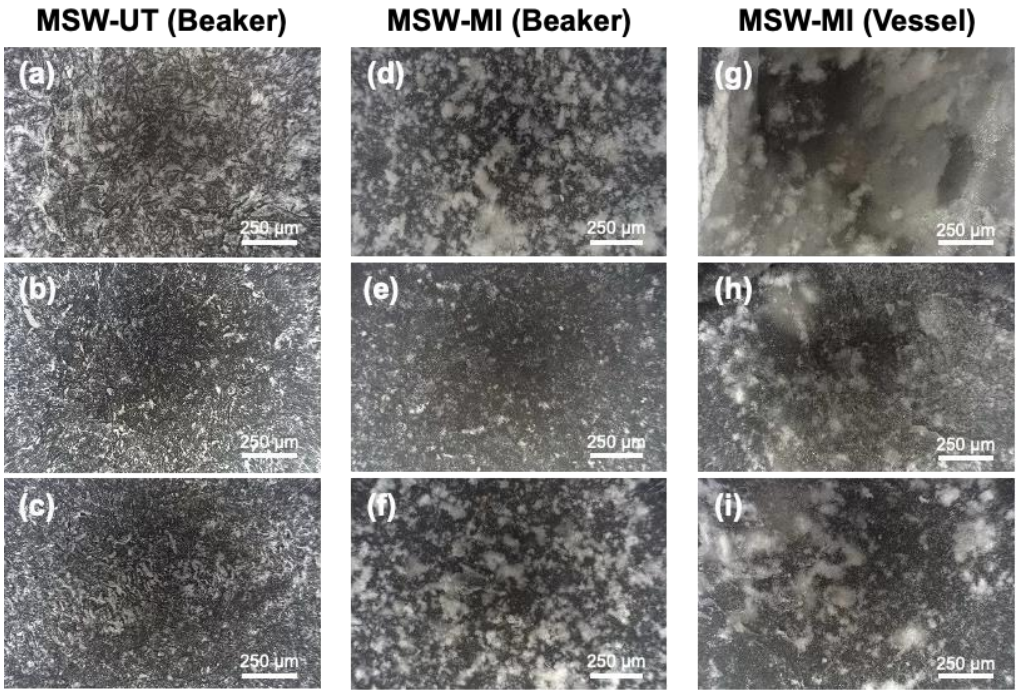

Supplementary Fig. 9. Optical microscope images of recovered polymers.
Textural and visual similarities in recovered polymers obtained from **a-c,** MSW-UT (beaker-scale), **d-f,** MSW-MI (beaker-scale), and **g-i,** MSW-MI (vessel-scale). Despite feedstock and process variations, the recovered polymers consistently exhibit comparable morphology, highlighting the reproducibility of STRAP.

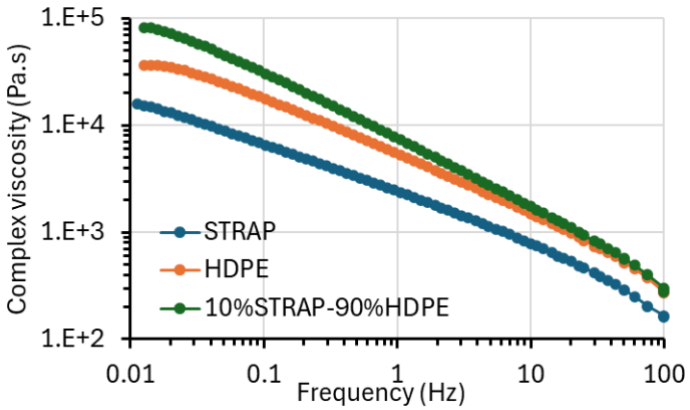

Supplementary Fig. 10. Complex viscosity versus frequency for STRAP-recovered polymer, virgin HDPE, and a 10 wt% STRAP-recovered polymer and 90 wt% virgin HDPE blend.

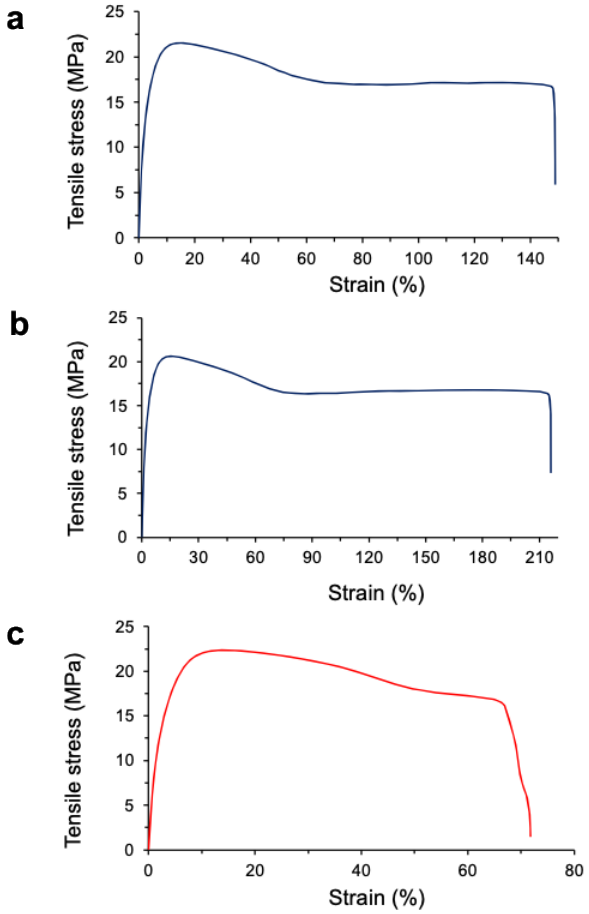

Supplementary Fig. 11. Representative tensile stress-strain curves of polymer samples.
a-b, Blended samples containing 10wt% STRAP-recovered polymer and 90wt% virgin HDPE. **c,** Virgin HDPE.

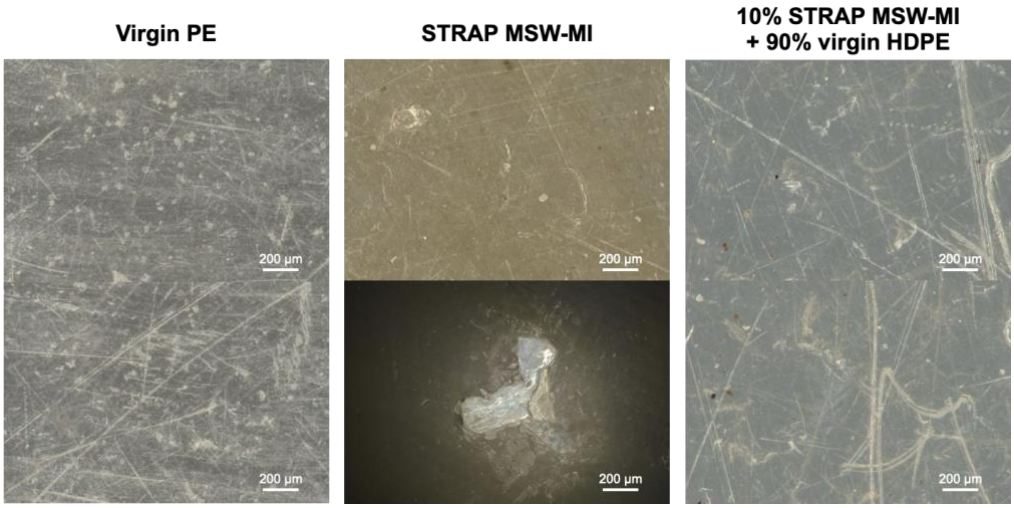

Supplementary Fig. 12. Optical microscope images of hot-compressed films produced from virgin and recovered polymers.

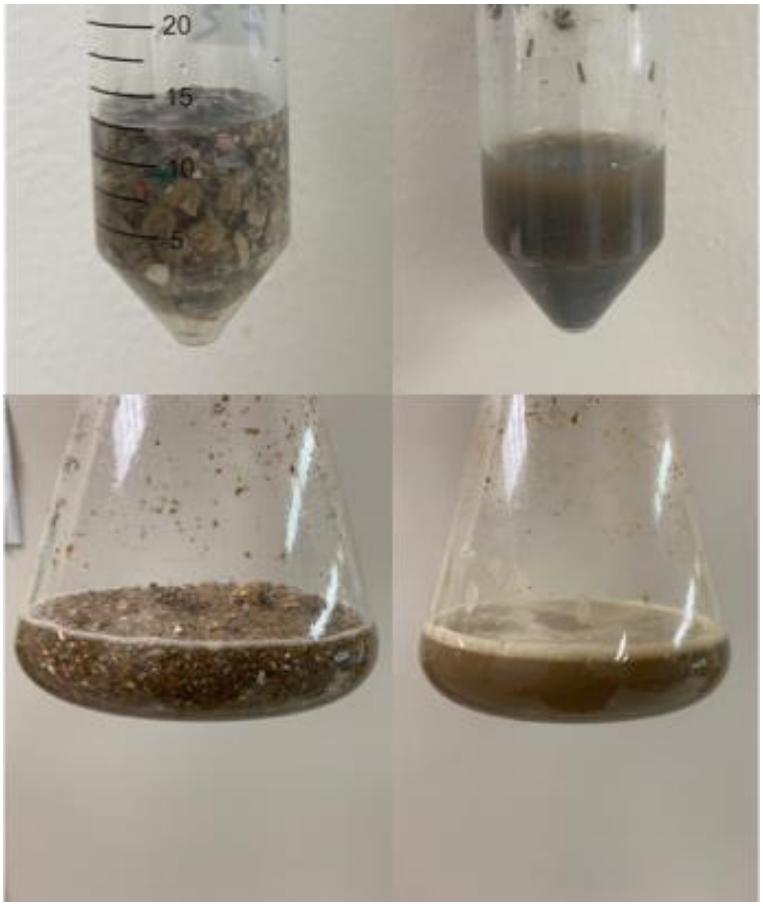

Supplementary Fig. 13. Images of MSW hydrolysates. 2 g (top) and 100 g (bottom) hydrolysates are pictured at the beginning (left) and end (right) of hydrolysis.

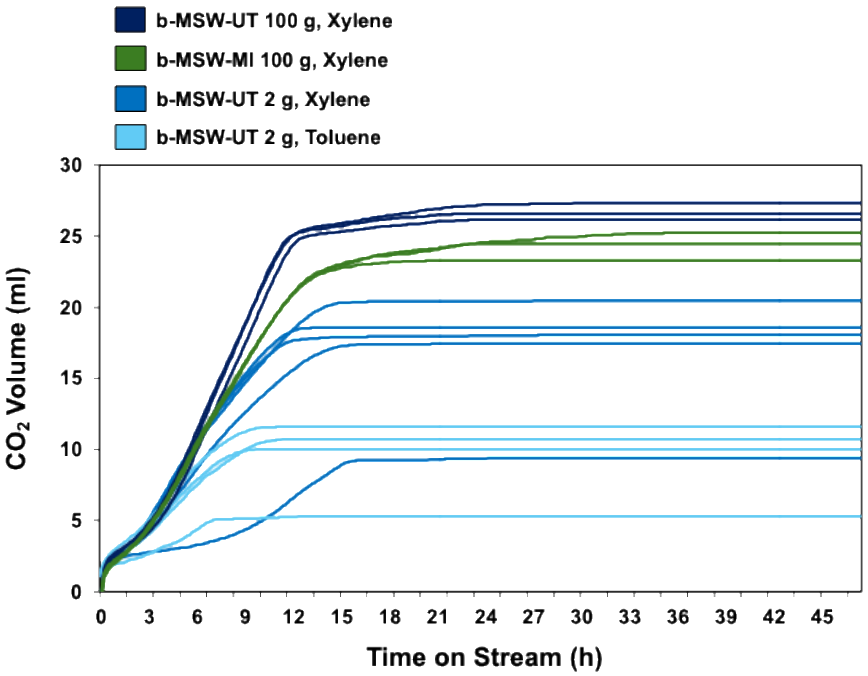

Supplementary Fig. 14. CO_2 volume measurements for fermentation experiments.
Hydrolysates from 2 g experiments were diluted 1-to-2 prior to fermentation. Fermentations of 100 g extracted MSW hydrolysates were conducted in technical triplicates on three separate days, and one representative replicate from each round of fermentation was selected for data analysis.

For fermentation rate calculations, CO_2 production was used as a proxy for ethanol production as CO_2 production is directly proportional to ethanol titer.

Supplementary Table 1. Calculated solubilities using COSMO-RS for PE and PP in some example solvents.

Solvent	T (°C)	PE solubility (wt%)	PP solubility (wt%)
p-Xylene	**120.0**	**38.6**	**38.3**
m-Xylene	**120.0**	**38.6**	**38.2**
o-Xylene	**120.0**	**37.8**	**37.2**
Dodecane	120.0	32.5	31.1
Toluene	109.6	22.6	30.9
Heptane	97.5	15.3	29.3
Cyclohexane	79.7	6.9	24.0
Triethylamine	88.0	8.7	23.2
Tetrahydropyran	87.0	7.3	20.9
Hexane	67.7	3.1	16.2
Cyclohexanol	120.0	22.1	14.7
2,3-Dihydropyran	85.0	5.0	14.4

Supplementary Table 2. Calculated solubility variations using COSMO-RS for LDPE, HDPE, PP-LMW[a], and PP-HMW[b] for different temperatures.

Solvent	T (°C)	Polymer solubility (wt%)			
		LDPE	HDPE	PP-LMW	PP-HMW
Xylene	25	0.05	0.00	1.09	0.03
	45	0.29	0.01	2.77	0.12
	65	1.26	0.08	6.32	0.50
	85	4.73	0.68	13.15	1.76
	105	16.02	4.67	24.89	5.37
	115	28.61	11.67	32.83	8.99
	125	49.31	28.57	41.90	14.64

[a] PP-LMW: polypropylene-low molecular weight, Mw 12,000 g·mol^{-1}
[b] PP-HMW: polypropylene-high molecular weight, Mw 250,000 g·mol^{-1}

Supplementary Table 3. Calculated solubilities using COSMO-RS for PS and PET in some solvent candidates.

Solvent	T (°C)	PS solubility (wt%)	PET solubility (wt%)
Toluene	109.6	41.0	2.5
THF	64	31.3	0.8
Tetrahydropyran	87	33.7	0.8
Styrene	120	41.9	4.8
N,N-Dimethylformamide	120	47.9	18.4
DMSO	120	18.2	8.3
GVL	**165**	**62.3**	**21.5**
Butyronitrile	116.6	45.7	17.6
Dichloroacetic Acid	120	9.6	17.1

Supplementary Table 4. STRAP-MSW-UT performance with toluene. STRAP experimental condition: Toluene 500 g, Temperature 110 ℃, Time 1 h.

Exp No.	Initial mass of MSW (g)	Recovered polyolefin (g)	Polyolefin yield (wt%)	Biogenic residue (g)	Overall Mass Balance (wt%)
1	15.02	1.60	10.66	11.54	87.49
2	15.07	1.51	10.03	10.89	82.27
3	15.10	1.68	11.12	12.10	91.23
4	15.12	1.83	12.13	12.20	92.85
5	15.12	1.68	11.09	12.09	91.05
6	15.08	1.61	10.67	11.59	87.55
7	15.12	1.73	11.43	12.45	93.79
8	15.13	1.80	11.92	12.99	97.75
9	15.06	1.64	10.92	11.85	89.60
10	15.07	1.66	11.04	11.99	90.59
Average	**15.09**	**1.67**	**11.1**	**12.0**	**90.4**
STDEV	**0.04**	**0.10**	**0.6**	**0.5**	**4.2**

Supplementary Table 5. STRAP-MSW-UT performance with xylene. STRAP experimental condition: Xylene 500 g, Temperature 130 ℃, Time 1 h.

Exp No.	Initial mass of MSW (g)	Recovered polyolefin (g)	Polyolefin yield (wt%)	Biogenic residue (g)	Overall mass balance (wt%)
1	15.03	2.52	16.76	12.08	97.16
2	15.10	2.61	17.31	11.61	94.20
3	15.11	2.46	16.26	11.03	89.34
4	15.24	2.37	15.54	11.86	93.43
5	15.05	2.52	16.78	11.27	91.69
6	15.10	2.53	16.77	11.80	94.93
7	15.14	2.63	17.39	11.52	93.52
8	15.17	2.72	17.91	11.55	94.06
9	15.14	2.50	16.50	11.60	93.18
10	15.21	2.58	16.96	12.04	96.11
Average	**15.13**	**2.54**	**16.8**	**11.6**	**93.7**
STDEV	**0.07**	**0.10**	**0.7**	**0.3**	**2.2**

Supplementary Table 6. Performance of the second STRAP stage using GVL on residues from the first STRAP stage with xylene. STRAP experimental condition: GVL 300 g, Temperature 170 ℃, Time 1 h.

Exp No.	Initial mass of MSW (g)	Recovered PET (g)	PET yield (wt%)	Biogenic residue (g)	Overall mass balance (wt%)
1	10.11	0.48	4.75	9.12	94.96
2	10.05	0.67	6.67	8.92	95.42
3	10.18	0.54	5.30	8.96	93.32
4	10.01	0.86	8.59	8.86	97.10
5	10.07	0.53	5.26	9.24	97.02
Average	**10.08**	**0.62**	**6.1**	**9.0**	**95.6**
STDEV	**0.06**	**0.15**	**1.6**	**0.2**	**1.6**

Supplementary Table 7. HS-GC analysis of recovered polymers.

Sample	TVOC (BP<100°C) (ppm)	TVOC (BP<200°C) (ppm)
MSW-UT_Xyl	19.1	39.6
MSW-UT_Tol	24.9	35.3

Supplementary Table 8. STRAP-MSW-MI performance with xylene. STRAP experimental condition: Xylene 500 g, Temperature 130 ℃, Time 1 h.

Exp No.	Initial mass of MSW (g)	Recovered polyolefin (g)	Polyolefin yield (wt%)	Biogenic residue (g)	Overall mass balance (wt%)
1	19.89	7.05	35.4	10.5	88.2
2	20.07	6.62	33.0	10.6	85.8
3	20.10	7.36	36.6	11.1	91.8
4	20.17	7.73	38.0	10.4	89.9
5	20.08	8.45	42.1	10.1	92.4
6	20.07	8.06	40.2	9.8	89.0
7	20.19	7.32	36.3	10.5	88.26
8	40.36	13.13	32.5	24.2	92.5
9	40.0	13.35	33.4	23.5	92.1
10	40.0	14.47	36.2	22.3	91.9
Average			**36.4**		**90.2**
STDEV			**3.1**		**2.3**

Supplementary Table 9. Scale-up experiments of STRAP-MSW-MI with xylene. STRAP experimental condition: Xylene 6000 g, Temperature 130 ℃, Time 3 h.

Exp No.	Initial mass of MSW (g)	Recovered polyolefin (g)	Polyolefin yield (wt%)	Biogenic residue (g)	Overall mass balance (wt%)
1	201.3	72.1775	35.9	111.4	91.2
2	201.4	70.2055	34.9	115.6	92.3
3	200.5	77.5449	38.7	109.2	93.1
4	200.4	79.4869	39.7	109.4	94.3
5	201.1	88.0146	43.8	103.9	95.4
Average			**38.6**		**93.3**
STDEV			**3.5**		**1.7**

Supplementary Table 10. Elemental composition of MSW-MI, biogenic residues after STRAP, recovered polyolefins, and virgin polymers.

Sample name	N (wt%)	C (wt%)	H (wt%)	S (wt%)	Ash (wt%)	O (wt%)[a]	H/C (atomic)[b]	H/C_{eff} (atomic)[b]
MSW-MI	0	53.1 ± 19.0	7.8 ± 3.7	0.1 ± 0.1	9.7 ± 0.9	29.3 ± 19.4	1.75	0.92
Biogenic residues after STRAP	0.05 ± 0.2	50.6 ± 8.6	5.9 ± 0.9	0.17 ± 0.05	15.5 ± 0.8	27.7 ± 8.7	1.39	0.54
Recovered polyolefin (STRAP with xylene)	0	84.3 ± 1.8	13.8 ± 0.8	0.3 ± 0.1	0.12 ± 0.03	≈0[c]	1.95	1.95
Virgin HDPE	0	85.6	14.1	0.3	0	0	1.96	1.96
Virgin PP	0	85.7	14.1	0.2	0	0	1.96	1.96
Virgin LDPE	0	86.2	13.7	0.1	0	0	1.89	1.89

[a] Oxygen content was calculated by difference (O = 100−(C+H+N+S+Ash)), and the associated uncertainty was estimated by error propagation ($\sigma 0 = \sqrt{\sigma C^2 + \sigma H^2 + \sigma N^2 + \sigma S^2 + \sigma Ash^2}$); values within the propagated uncertainty of zero are reported as ≈0.

[b] H/C and H/C_{eff} were computed from elemental wt% as atomic ratios; $H/C = n_H/n_C$; $H/C_{eff} = (n_H\text{-}2\cdot n_O\text{-}3\cdot n_N\text{-}2\cdot n_S)/n_C$

[c] O = 1.48 ± 1.97 wt% ≈ 0 wt%; within error, consistent with oxygen-free polyolefin.

Supplementary Table 11. Compositional analysis of MSW. The results reflect the composition of material used in 2 g hydrolysis experiments. Standard errors are shown for n = 3 replicates.

	Pre-processed MSW		**Biogenic residues after STRAP with xylene**		**Biogenic residues after STRAP with toluene**
	MSW-UT (wt%)	**MSW-MI (wt%)**	**MSW-UT (wt%)**	**MSW-MI (wt%)**	**MSW-UT (wt%)**
CH_2Cl_2 extractives	8.64	8.96			
Klason Lignin	38.2 ± 0.7	14.6 ± 0.1	57.1 ± 1.0	20.7 ± 0.2	34.9 ± 1.8
Acid soluble lignin	0.9 ± 0.05	0.5 ± 0.1	1.7 ± 0.25	0.6 ± 0.1	1.8 ± 0.04
Glucan	22.5 ± 0.9	34.2 ± 0.6	31.3 ± 0.1	33.7 ± 0.1	31.3 ± 0.1
Xylan	3.3 ± 0.3	7.2 ± 0.9	5.2 ± 0.1	6.8 ± 1.2	5.2 ± 0.1
Galactan	0.6 ± 0.7	0.7 ± 0.1	0.9 ± 0.02	-	0.6 ± 0.02
Mannan	1.8 ± 0.3	4.13 ± 0.3	3.3 ± 0.3	5.6 ± 0.2	2.0 ± 0.1
Total Carbohydrate	28.2	46.23	40.7	46.1	39.1
Ash	10.6 ± 1.0	10.4 ± 1.5	13.8 ± 0.6	11.2 ± 0.4	
Colorimetric analyses					
Acetyl bromide lignin	31.6 ± 9.0	35 ± 8.0	33.6 ± 3.0	31.6 ± 1.0	
Total carbohydrate (phenol-sulfuric)	60.1 ± 1.83	51.8 ± 6.3	59.7 ± 6.2	52.0 ± 3.9	

Supplementary Table 12. Compositional analysis of MSW. The results reflect the composition of material used in 10 and 100 g hydrolysis experiments.

	Material (Origin, STRAP solvent)	**b-MSW (UT, xylene)**	**b-MSW (UT, xylene)**	**b-MSW (MI, xylene)**	**b-MSW (MI, xylene)**
	%Whole Ash	10.85	11.15	9.91	11.28
	%Structural Ash	10.96	9.19	8.63	10.33
%H_2O Extractives	%Extractable Inorganics	0.22	2.26	1.3	1.3
	%H_2O Extractives	2.6	2.93	2.29	2.37
%H_2O Extractives	%NS Glucan	1.01	0.87	0.79	0.87
	%NS Xylan	0.12	0.19	0.15	0.13
	%NS Galactan	0.1	0.1	0.12	0.11
	%NS Arabinan	0	0.05	0	0
	%NS Mannan	0.03	0.03	0.04	0.03
	%Water Extractives Others	1.11	0.85	0.66	0.69
	%EtOH Extractives	0.46	0.75	0.66	0.58
	%Total Extractives	3.06	3.68	2.95	2.95
	%Lignin	28.81	23.34	40.38	37.05
	%Lignin (Acid Insoluble)	26.18	20.52	38.26	34.64
	%Lignin (Acid Soluble)	2.63	2.82	2.11	2.41
	%Glucan	42.85	48.35	36.13	37.7

	%Xylan	7.88	7.99	6.56	6.83
	%Galactan	0.86	0.78	0.95	0.89
	%Arabinan	0	0	0	0
	%Mannan	3.06	4.07	2.69	2.7
	%Acetate	0.29	0.33	0.29	0.28
	%Total	97.75	99.1	99.29	99.47

Supplementary Table 13. Preliminary hydrolysis results and microbial growth from samples without kanamycin. Images shown are agar plates incubated for one week. Fermentable sugar yield results are shown for n = 3 replicates. Glucose and xylose yields were measured via HPLC. DNA amplicon sequencing was used to identify the microbial colonies at the genus level. Colony #2 from the b-MSW (UT, toluene) hydrolysate was not identified.

Material (Origin, STRAP solvent) and image of LB agar plate	**Fermentable sugar concentration (mg/mL)**	**Colony #**	**Genus of colony microbes**
MSW-UT 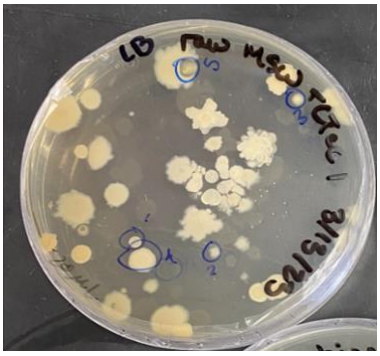	13.5 ± 0.7	1	*Bacillus*
		2	*Alkalihalobacillus*
		3	*Weizmannia, Penicillium*
		4	*Bacillus*
		5	*Bacillus*
b-MSW (UT, toluene) 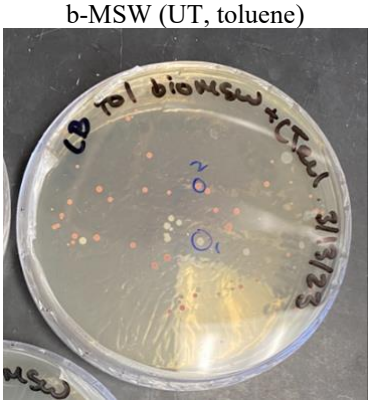	9.3 ± 1.7	1	*Weizmannia*
b-MSW (UT, xylene) 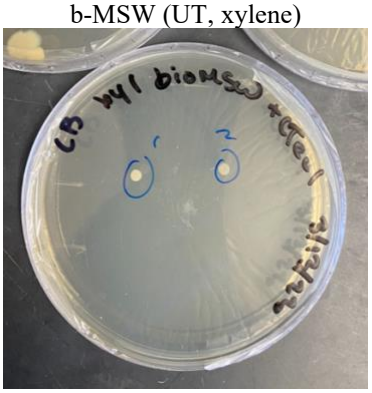	17.5 ± 3.1	1	*Weizmannia*
		2	*Penicillium*

MSW hydrolysates were plated on non-selective Lysogeny Broth (LB) agar and fungi-selective Potato Dextrose Agar (PDA) supplemented with chloramphenicol to assess microbial

carryover. After one week, no colonies were observed on PDA, whereas LB plates showed substantial bacterial growth for the MSW-UT and b-MSW (UT, toluene) hydrolysates (~30 colonies), but only two colonies for the b-MSW (UT, xylene) hydrolysate. This trend is consistent with the higher fermentable sugar concentration measured for the xylene-derived b-MSW hydrolysate and suggests that the higher STRAP temperature used with xylene reduced viable microbial load relative to toluene.

Table S14. End product analysis results for all biogenic MSW hydrolysates. Hydrolysates from 2 g experiments were diluted 1:2 prior to end product analysis. Hydrolysis reactions without CTec added are included as controls.

MSW mass (g)	Buffer added for hydrolysis (mL)	MSW source	Solvent	Treatment	CTec added for hydrolysis (mL)	Replicate #	Acetate (g/L)	Ethanol (g/L)	Formate (g/L)	Glucose (g/L)	Glycerol (g/L)	Lactate (g/L)	Pyruvate (g/L)	Succinate (g/L)	Xylitol (g/L)	Xylose (g/L)	Cellobiose (g/L)
2	9	Utah	Xylene	Kanamycin	1	1	1.04	0.00	0.00	20.37	0.03	2.10	0.00	0.06	0.04	3.38	0.27
2	9	Utah	Xylene	Kanamycin	1	2	0.99	0.05	0.04	9.82	0.02	10.93	0.03	0.10	0.02	3.69	0.07
2	9	Utah	Xylene	Kanamycin	1	3	0.68	0.00	0.07	21.39	0.07	0.19	0.00	0.04	0.02	3.52	0.37
2	9	Utah	Xylene	Kanamycin	1	4	0.69	0.00	0.06	23.75	0.06	0.17	0.00	0.04	0.02	3.66	0.47
2	9	Utah	Xylene	Kanamycin	1	5	1.13	0.00	0.00	19.36	0.04	1.17	0.00	0.05	0.02	3.48	0.26
2	9	Utah	Xylene	Kanamycin	0	1	0.70	0.00	0.07	0.04	0.00	0.27	0.05	0.03	0.03	0.08	0.04
2	9	Utah	Xylene	Kanamycin	0	2	0.69	0.00	0.06	0.02	0.06	0.20	0.02	0.01	0.04	0.01	0.08
2	9	Utah	Xylene	Kanamycin	0	3	0.69	0.00	0.05	0.10	0.05	0.19	0.01	0.01	0.04	0.02	0.08
2	9	Utah	Xylene	Kanamycin	0	4	0.49	0.00	0.00	0.06	0.01	0.16	0.02	0.01	0.04	0.00	0.01

2	9	Utah	Xylene	Kanamycin	0	5	0.62	0.00	0.04	0.13	0.05	0.19	0.01	0.01	0.05	0.03	0.02
2	9	Utah	Toluene	Kanamycin	1	1	0.67	0.00	0.11	11.50	0.04	0.10	0.00	0.03	0.04	2.28	0.19
2	9	Utah	Toluene	Kanamycin	1	2	0.64	0.01	0.09	10.78	0.04	0.10	0.00	0.03	0.04	2.12	0.21
2	9	Utah	Toluene	Kanamycin	1	3	0.66	0.01	0.11	11.37	0.04	0.12	0.00	0.03	0.04	2.30	0.16
2	9	Utah	Toluene	Kanamycin	1	4	1.23	0.13	0.02	3.84	0.00	7.68	0.00	0.05	0.04	2.37	0.16
2	9	Utah	Toluene	Kanamycin	0	1	0.62	0.00	0.11	0.13	0.03	0.11	0.01	0.02	0.06	0.02	0.01
2	9	Utah	Toluene	Kanamycin	0	2	0.64	0.00	0.10	0.16	0.03	0.13	0.01	0.02	0.05	0.04	0.01
2	9	Utah	Toluene	Kanamycin	0	3	0.58	0.03	0.02	0.01	0.01	0.10	0.01	0.01	0.06	0.01	0.00
2	9	Utah	Toluene	Kanamycin	0	4	0.63	0.00	0.11	0.03	0.03	0.10	0.01	0.02	0.06	0.01	0.02
2	9	Utah	Toluene	Kanamycin	0	5	0.64	0.00	0.11	0.03	0.03	0.11	0.01	0.02	0.06	0.01	0.02
0	9			Kanamycin	1	1	0.60	0.02	0.00	1.80	0.01	0.00	0.00	0.01	0.07	0.10	0.26
0	9			Kanamycin	1	2	0.52	0.00	0.07	1.57	0.00	0.06	0.00	0.01	0.08	0.09	0.23

0	9			Kanamycin	1	3	0.57	0.00	0.01	1.67	0.01	0.00	0.00	0.00	0.06	0.09	0.27
10	100	Utah	Xylene	None	5	1	2.59	0.00	0.00	10.71	0.00	7.47	0.00	0.16	0.00	3.36	2.06
10	100	Utah	Xylene	Kanamycin	5	1	0.93	0.00	0.00	24.09	0.00	0.00	0.00	0.00	0.09	3.51	2.93
10	100	Utah	Xylene	Steam	5	1	0.71	0.00	0.00	25.30	0.00	0.00	0.00	0.00	0.00	3.13	3.25
100	1000	Utah	Xylene	Kanamycin	50	1	0.79	0.00	0.00	23.00	0.00	9.60	0.00	0.16	0.00	5.40	2.32
100	1000	Utah	Xylene	Kanamycin	50	1	1.87	0.00	0.41	21.01	0.00	3.00	0.00	0.12	0.11	3.09	3.34

Table S15. Enzymatic hydrolysis of b-MSW. Glucose and xylose concentrations were measured via HPLC. Fermentable sugar titers and yields represent the combined values of glucose and xylose. Standard errors are shown for 2 g experiments (n = 4 for b-MSW (Toluene), n = 5 for b-MSW (Xylene)).

Material (Origin, STRAP solvent, Mass)	Initial solids-to-liquid ratio (w/v)	Volume of recovered hydrolysate (mL)	Sugar type	Titer ($g \cdot L^{-1}$)	Yield from biogenic MSW (w/w)[b]	Saccharification yield[b]
b-MSW (UT, Toluene, 2 g)	1:5	10[a]	Glucose	15.4 ± 3.3	7.7% ± 1.7%	24.6% ± 5.4%
			Xylose	4.3 ± 1.4	2.2% ± 0.0%	41.8% ± 1.7%
			Fermentable sugars	19.7 ± 3.4	9.9% ± 1.7%	27.4% ± 4.7%
b-MSW (UT, Xylene, 2 g)	1:5	10[a]	Glucose	34.5 ± 4.4	17.3% ± 2.2%	55.1% ± 7.2%
			Xylose	6.9 ± 0.1	3.5% ± 0.1%	66.4% ± 2.3%
			Fermentable sugars	41.4 ± 4.5	20.7% ± 2.2%	57.0% ± 6.4%
b-MSW (UT, Xylene, 100 g)	2:21	760	Glucose	21.4	16.3%	35.7%
			Xylose	5.3	4.0%	50.9%
			Fermentable sugars	26.7	20.3%	38.3%
b-MSW (MI, Xylene, 100 g)	2:21	850	Glucose	19.4	16.5%	44.7%
			Xylose	3.0	2.6%	38.1%
			Fermentable sugars	22.4	19.1%	43.5%

[a] Yields from 2 g experiments were calculated assuming an initial hydrolysate volume of 10 mL and a 2× dilution.
[b] Values for 100 g experiments were corrected using CTec-only controls from 2 g experiments, scaled to match enzyme-to-liquid ratios.

Initial hydrolysis trials used 2 g of STRAP-derived b-MSW (MSW-UT) at a 1:5 solids-to-liquid ratio. Fermentable sugar titers (glucose + xylose) were calculated by subtracting CTec-only background contributions from enzyme-treated samples (Supplementary Method 4, Eq.

1). Because hydrolysis was sampled at a single time point (72 h), saccharification rates were not determined; instead, yields were calculated from measured titers, hydrolysate volume, and initial biomass mass (Supplementary Method 4, Eq. 2-3). For the 2 g experiments, yields were calculated assuming an initial hydrolysate volume of 10 mL (footnote a), giving fermentable sugar yields of 20.7% (xylene) and 9.9% (toluene). Saccharification yields were estimated using the measured glucan and xylan contents of b-MSW (Supplementary Tables 12 and 13), yielding 57.0% for xylene-derived residues and 27.4% for toluene-derived residues. Overall, xylene-derived b-MSW consistently showed higher sugar release, and xylan conversion exceeded glucan conversion.

Supplementary Table 16. Effect of kanamycin and steam sterilization on hydrolysis. Fermentable sugar concentrations (glucose + xylose) were measured by HPLC. Yields were calculated using adjusted CTec-only controls from 2 g hydrolysis experiments.

Material (Origin, STRAP solvent)	Mass of biogenic MSW (g)	Volume of recovered hydrolysate (mL)	Treatment	Fermentable sugar titer ($g \cdot L^{-1}$)	Fermentable sugar yield from biogenic MSW (w/w)	Fermentable sugar saccharification yield
b-MSW (UT, Xylene)	10	86	None	12.4	10.7%	20.4%
		88	Kanamycin	25.9	22.9%	42.6%
		75	Steam	26.7	20.2%	37.4%

Steam sterilization was evaluated as an antibiotic-free post-STRAP conditioning step to mitigate microbial contamination during enzymatic hydrolysis of xylene-derived b-MSW. Supplementary Table 16 compares 10 g hydrolysis trials performed with no treatment, kanamycin addition, or steam sterilization. Steam and kanamycin produced similar fermentable sugar titers (26.7 and 25.9 $g \cdot L^{-1}$), yields (20.2% and 22.9%), and saccharification yields (37.4% and 42.6%), whereas the untreated condition gave substantially lower sugar recovery (12.4 $g \cdot L^{-1}$; 10.7% yield; 20.4% saccharification yield). End-product profiles (Supplementary Table 18) are consistent with microbial activity in the untreated sample, supporting the interpretation that simple steam sterilization can stabilize hydrolysis performance without antibiotics.

Supplementary Table 17. End product analysis results for fermentation of all biogenic MSW hydrolysates. Hydrolysates from 2 g experiments were diluted 1-to-2 prior to fermentation. Fermentations of 100 g extracted MSW hydrolysates were conducted in technical triplicates on three separate days, and one representative replicate from each round of fermentation was selected for data analysis. Hydrolysis reactions without CTec added are included as controls.

MSW mass (g)	Buffer added for hydrolysis (mL)	MSW source	Solvent	Hydrolysis treatment	CTec added for hydrolysis (mL)	Replicate #	Acetate (g/L)	Ethanol (g/L)	Formate (g/L)	Glucose (g/L)	Glycerol (g/L)	Lactate (g/L)	Pyruvate (g/L)	Succinate (g/L)	Xylitol (g/L)	Xylose (g/L)	Cellobiose (g/L)
2	9	Utah	Xylene	Kanamycin	1	1	0.67	8.80	0.00	0.13	1.36	1.65	0.06	0.23	0.07	0.88	0.20
2	9	Utah	Xylene	Kanamycin	1	2	0.66	4.28	0.03	0.23	0.50	9.69	0.09	0.12	0.05	1.33	0.07
2	9	Utah	Xylene	Kanamycin	1	3	0.53	9.55	0.02	0.22	1.41	0.16	0.05	0.16	0.07	0.46	0.25
2	9	Utah	Xylene	Kanamycin	1	4	0.48	10.10	0.02	0.19	1.39	0.14	0.04	0.17	0.02	0.82	0.35
2	9	Utah	Xylene	Kanamycin	1	5	0.89	8.59	0.00	0.18	1.20	0.95	0.08	0.20	0.02	0.52	0.19
2	9	Utah	Xylene	Kanamycin	0	1	0.10	0.07	0.06	0.11	0.00	0.10	0.07	0.01	0.06	0.03	0.04
2	9	Utah	Xylene	Kanamycin	0	2	0.02	0.00	0.06	0.13	0.06	0.05	0.05	0.02	0.07	0.00	0.08
2	9	Utah	Xylene	Kanamycin	0	3	0.13	0.00	0.05	0.13	0.05	0.04	0.04	0.01	0.07	0.01	0.05
2	9	Utah	Xylene	Kanamycin	0	4	0.01	0.05	0.00	0.06	0.01	0.15	0.02	0.03	0.02	0.01	0.01

2	9	Utah	Xylene	Kanamycin	0	5	0.02	0.01	0.05	0.05	0.06	0.05	0.05	0.01	0.02	0.02	0.03
2	9	Utah	Toluene	Kanamycin	1	1	0.45	4.80	0.06	0.23	0.89	0.01	0.00	0.13	0.08	0.55	0.16
2	9	Utah	Toluene	Kanamycin	1	2	0.36	4.42	0.05	0.23	0.75	0.03	0.01	0.10	0.07	0.46	0.12
2	9	Utah	Toluene	Kanamycin	1	3	0.40	4.50	0.05	0.18	0.74	0.06	0.02	0.11	0.03	0.74	0.18
2	9	Utah	Toluene	Kanamycin	1	4	0.90	1.99	0.02	0.05	0.23	6.88	0.05	0.07	0.03	0.18	0.13
2	9	Utah	Toluene	Kanamycin	0	1	0.00	0.02	0.11	0.13	0.04	0.01	0.02	0.02	0.08	0.01	0.01
2	9	Utah	Toluene	Kanamycin	0	2	0.08	0.03	0.10	0.12	0.04	0.02	0.02	0.02	0.08	0.02	0.01
2	9	Utah	Toluene	Kanamycin	0	3	0.00	0.00	0.01	0.08	0.01	0.02	0.01	0.01	0.10	0.00	0.01
2	9	Utah	Toluene	Kanamycin	0	4	0.11	0.02	0.11	0.07	0.04	0.02	0.03	0.03	0.04	0.01	0.01
2	9	Utah	Toluene	Kanamycin	0	5	0.03	0.00	0.07	0.06	0.02	0.02	0.02	0.02	0.04	0.01	0.02
0	9			Kanamycin	1	1	0.05	0.30	0.00	0.18	0.09	0.00	0.00	0.01	0.06	0.00	0.21
0	9			Kanamycin	1	2	0.11	0.17	0.01	0.23	0.07	0.00	0.01	0.00	0.07	0.00	0.20
0	9			Kanamycin	1	3	0.09	0.33	0.00	0.08	0.13	0.01	0.00	0.01	0.04	0.01	0.21

100	1000	Utah	Xylene	Kanamycin	50	1	0.75	11.84	0.00	0.00	1.83	9.10	0.00	0.21	0.04	0.24	2.11
100	1000	Utah	Xylene	Kanamycin	50		0.63	11.66	0.00	0.00	1.73	8.93	0.00	0.16	0.00	0.00	2.10
100	1000	Utah	Xylene	Kanamycin	50		0.61	14.04	0.00	0.00	2.08	10.65	0.02	0.17	0.05	0.21	2.51
100	1000	Utah	Xylene	Kanamycin	50		0.78	11.56	0.00	0.00	1.78	8.88	0.00	0.19	0.05	0.20	2.07
100	1000	Utah	Xylene	Kanamycin	50	2	0.86	11.76	0.00	0.00	1.82	9.03	0.00	0.20	0.00	0.00	2.10
100	1000	Utah	Xylene	Kanamycin	50		0.74	11.83	0.00	0.04	1.82	9.02	0.00	0.17	0.06	0.17	2.12
100	1000	Utah	Xylene	Kanamycin	50		0.75	11.77	0.00	0.00	1.76	8.99	0.00	0.22	0.08	0.20	2.09
100	1000	Utah	Xylene	Kanamycin	50		0.62	11.66	0.00	0.00	1.72	8.89	0.00	0.20	0.00	0.00	2.08
100	1000	Utah	Xylene	Kanamycin	50	3	0.85	13.35	0.00	0.05	2.02	10.10	0.03	0.17	0.04	0.23	2.38
100	1000	Michigan	Xylene	Kanamycin	50	1	1.61	12.10	0.33	0.19	1.55	2.89	0.17	0.34	0.14	0.36	0.48
100	1000	Michigan	Xylene	Kanamycin	50		1.55	12.07	0.35	0.18	1.62	3.01	0.18	0.35	0.11	0.36	0.54
100	1000	Michigan	Xylene	Kanamycin	50		1.68	11.97	0.34	0.17	1.54	2.91	0.16	0.31	0.00	0.33	0.50
100	1000	Michigan	Xylene	Kanamycin	50		1.65	12.25	0.35	0.13	1.59	2.85	0.12	0.33	0.13	0.34	0.44

100	1000	Michigan	Xylene	Kanamycin	50	2	1.73	11.83	0.31	0.15	1.58	2.80	0.00	0.32	0.11	0.33	0.42
100	1000	Michigan	Xylene	Kanamycin	50		1.77	12.12	0.30	0.17	1.65	2.84	0.00	0.32	0.14	0.36	0.44
100	1000	Michigan	Xylene	Kanamycin	50		1.55	11.32	0.35	0.13	1.59	2.80	0.12	0.34	0.10	0.33	0.54
100	1000	Michigan	Xylene	Kanamycin	50		1.53	11.43	0.35	0.13	1.60	2.86	0.13	0.34	0.12	0.30	0.50
100	1000	Michigan	Xylene	Kanamycin	50	3	1.51	11.26	0.32	0.13	1.54	2.74	0.14	0.34	0.11	0.38	0.50

Supplementary Table 18. Fermentation of b-MSW hydrolysates. Ethanol titers, fermentation rates, and process yields were measured for 2 g and 100 g hydrolysates using *Saccharomyces cerevisiae* GLBRCY1384. Fermentation rate was determined based on the time of peak CO_2 evolution. Theoretical ethanol yields were calculated with or without correction for cellobiose consumption, as noted. Standard errors are shown for 2 g experiments (n = 4 for toluene, n = 5 for xylene) and for 100 g experiments (n = 3 technical replicates).

Material (Origin, STRAP solvent)	Mass of biogenic MSW (g)	Ethanol titer ($g \cdot L^{-1}$)	Fermentation rate (mg ethanol$\cdot L^{-1} \cdot h^{-1}$)	Ethanol theoretical process yield from fermentation	Ethanol yield from MSW (w/w)	Ethanol theoretical process yield from hydrolysis and fermentation (w/w)
b-MSW (UT, Toluene)	2	3.7 ± 0.6	336.1 ± 58.9	65.7% ± 1.1%	3.7% ± 0.6%[a]	19.1% ± 42.2%[a]
b-MSW (UT, Xylene)	2	8.0 ± 0.9	532.0 ± 67.8	71.2% ± 2.1%	8.0% ± 0.9%[a]	41.7% ± 15.2%[a]
b-MSW (UT, Xylene)	100	12.1 ± 0.4	543.1 ± 26.7	85.0% ± 2.9%	9.2% ± 0.3%[b]	32.5%[b]
b-MSW (MI, Xylene)	100	11.5 ± 0.2	523.2 ± 43.2	74.7% ± 1.3%[c]	9.8% ± 0.1%[b]	42.4%[b]

[a] Yields from 2 g experiments were calculated assuming an initial hydrolysate volume of 10 mL and a 2× dilution.
[b] Values for 100 g experiments were corrected using CTec-only controls from 2 g experiments, scaled to match enzyme-to-liquid ratios.
[c] Adjusted for cellobiose consumption during fermentation (Supplementary Method 4, Eq. 6).

Supplementary Table 19. Comparison of established and emerging MSW handling/valorization pathways and key advantages/limitations relative to STRAP-MSW

Pathway	Primary objective	Typical severity / unit ops [a]	Tolerance to MSW heterogeneity & contaminants [a]	Main products	Key bottlenecks (MSW-relevant)	Circularity / value retention [a]	Scale / implementation risk notes
Landfilling	Disposal	Low; long residence time; minimal processing	High (broad acceptance of mixed wastes)	Landfill Gas (LFG; CH_4/CO_2), leachate	Methane emissions, long-term monitoring, loss of recoverable material value	Low	Mature; increasingly constrained by environmental and policy considerations
Incineration / Waste-to-Energy (WtE)	Volume reduction + energy	High T oxidation (~800-1000 °C); air-pollution control required	Medium-High (accepts mixed MSW; performance depends on APC)	Electricity/steam ; bottom ash and fly ash	Emissions control; ash handling; destroys polymer molecular value	Low-Medium	Mature; strong siting and regulatory constraints
Mechanical recycling	Materials recycling (selected fractions)	Low-medium; sorting, washing, size reduction, remelting	Low (sensitive to mixing, soiling, multilayers)	Regrind/pellets	Incompatibility and contamination; property loss and downcycling	Medium (for clean single-polymer streams)	Mature for bottles/rigid streams; limited for films and mixed MSW plastics
Pyrolysis (plastic-to-oil)	Fuels/chemical feedstocks	High T (~300-760 °C); product upgrading typically required	Medium (can accept mixed plastics; sensitive to PVC, metals, and moisture)	Pyrolysis oil, gas, char	Halogens and heteroatoms; complex product slate; upgrading and catalyst deactivation	Medium (often energy pathway; degree of circularity depends on upgrading and product use)	Scale-up depends on feed specification control and reliable upgrading integration
Gasification (syngas)	Syngas → fuels and chemicals	Very high T (~700-1500 °C); extensive gas cleanup	Medium (heterogeneity and moisture remain major challenges)	Syngas	Tar/slag management; gas cleanup; high capital expenditure; reliability and uptime	Medium (contingent on efficient syngas upgrading)	First-of-a-Kind risk can be high; end-to-end integration, yield, and uptime are critical

MBT (mechanical-biological treatment)	Stabilize organics + recover recyclables	Medium; mechanical sorting plus anaerobic digestion/composting	Medium (strongly feed- and market-dependent)	Compost/digestate, biogas, recovered recyclables	Variable performance; recovered materials often limited purity/value	Medium	Commercially deployed; outcomes depend on local composition and offtake markets
STRAP-MSW (this work)	Selective fractionation + co-valorization	Low-Medium (~110-140 °C); filtration and precipitation; solvent recovery	Medium-High (designed to handle mixed/contaminated polymer fractions)	Polymer resins (PE/PP blend); biogenic residue to sugars/ethanol	Solvent management (EHS and recovery); separation logistics; residue variability	High (polymer molecular value retained; co-valorization of carbohydrate fraction)	Demonstrated solvent recycle and scale-up with mass balance/accountability in this study

[a] Relative process severity, feedstock robustness, and circularity/value retention are heuristic qualitative descriptors assigned for high-level cross-pathway comparison. These descriptors are literature-informed but are not derived from a formal TEA/LCA or standardized scoring framework.

1. Landfilling.

Landfilling remains one of the most widely used MSW management strategies in the United States and globally, largely due to low cost and operational simplicity. However, this linear disposal route carries long-term environmental liabilities. Anaerobic degradation of the organic fraction generates landfill gas (LFG), composed primarily of methane (CH_4) and carbon dioxide (CO_2)[1]. Methane has a substantially higher global warming potential than CO_2 over a 100-year horizon, and additional burdens include long-term leachate management and site monitoring. Landfilling also represents a permanent loss of recoverable polymeric and biogenic material value.

2. Incineration and waste-to-energy (WtE).

Incineration (waste-to-energy, WtE) oxidizes MSW at high temperatures (typically ~800-1000 °C) to reduce waste volume and generate steam and electricity[2–4]. While WtE can reduce reliance on landfilling, combustion of heterogeneous waste leads to complex emissions (NO_x, SO_x, dioxins/furans, and trace metals) and therefore requires robust air-pollution-control systems. Solid residues (bottom ash and fly ash) also require

management, with fly ash often treated as hazardous. From a circularity standpoint, WtE irreversibly converts both polymeric and biogenic fractions into low-value energy rather than recoverable materials.

3. Mechanical recycling.

Mechanical recycling relies on sorting, washing, size reduction, and remelting without changing polymer chemistry. For clean, single-polymer streams (e.g., PET bottles, HDPE containers), it can reduce energy use and greenhouse gas emissions relative to virgin polymer production. However, repeated thermal–mechanical processing can degrade polymer properties, often resulting in downcycling[5]. More importantly for MSW, mechanical recycling is highly sensitive to contamination, polymer incompatibility, and multilayer/composite packaging, which limits applicability to mixed plastics and flexible films commonly present in MSW[6].

4. Chemical recycling: pyrolysis, depolymerization, and gasification.

Chemical recycling encompasses thermal, catalytic, and solvent-enabled routes that convert plastics into fuels, chemical intermediates, or monomers[7]. These approaches can tolerate more heterogeneous feeds than mechanical recycling but often face challenges related to energy intensity, catalyst deactivation, product separation, and uncertain life-cycle performance depending on assumptions and system boundaries.

Pyrolysis decomposes polymers in the absence of oxygen (typically ~300-760 °C) to yield gases, char, and a complex liquid oil that may require upgrading; contaminants such as PVC can generate HCl, while nitrogen-containing species can complicate downstream processing[5].

Depolymerization can enable closed-loop recycling for condensation polymers such as PET[8,9], but is generally ineffective for polyolefins and remains sensitive to additives and mixed feeds typical of MSW.

Gasification converts carbonaceous waste to syngas (CO/H_2; typically ~700-1500 °C) that can be upgraded to fuels and chemicals[10,11]. For plastic-rich MSW, tar formation, feed heterogeneity, and capital intensity remain significant barriers. Plasma gasification can, in principle, process highly heterogeneous feeds and produce syngas along with vitrified slag[12,13], but high energy demand and cost have limited widespread deployment relative to established pathways.

5. Mechanical-biological treatment (MBT) and enzymatic recycling.

MBT integrates mechanical sorting with biological stabilization (e.g., composting or anaerobic digestion) to reduce landfill mass and recover recyclables[14]. However, recovered materials can be variable in purity and market value, and overall performance is strongly feedstock-dependent. Enzymatic recycling has also advanced as a low-severity route for selected polymers, particularly PET, enabling depolymerization under mild aqueous conditions[15]. Despite progress, enzymatic approaches currently face limitations for MSW applications, including kinetics, inhibition by additives/contaminants, and limited relevance to polyolefins and mixed plastic streams[16].

6. STRAP vs. Other MSW Handling Processes

STRAP is a selective fractionation strategy intended to address limitations of conventional MSW pathways. Unlike landfilling and incineration, which primarily dispose of material value, STRAP targets recovery of polymer resins while maintaining properties suitable for reuse. In contrast to mechanical recycling, which is constrained by contamination and polymer incompatibility, STRAP leverages polymer–solvent thermodynamics to separate polymers and remove dyes, adhesives, and organic residues that commonly drive downcycling. Relative to thermochemical conversion (e.g., pyrolysis and gasification), STRAP typically operates at lower temperatures (often ~110-140 °C), avoiding complex product mixtures that require extensive upgrading. In the integrated STRAP–MSW framework, polymer recovery is coupled to downstream processing of the remaining biogenic fraction for enzymatic hydrolysis and fermentation, enabling co-production of recycled polymers and bioethanol. The accompanying techno-economic and life-cycle analyses quantify the resulting performance relative to conventional fossil-derived polymers and established biofuel benchmarks.

Materials and Methods

Supplementary Method 1. Pre-treatment of raw-MSW, and Chemicals.

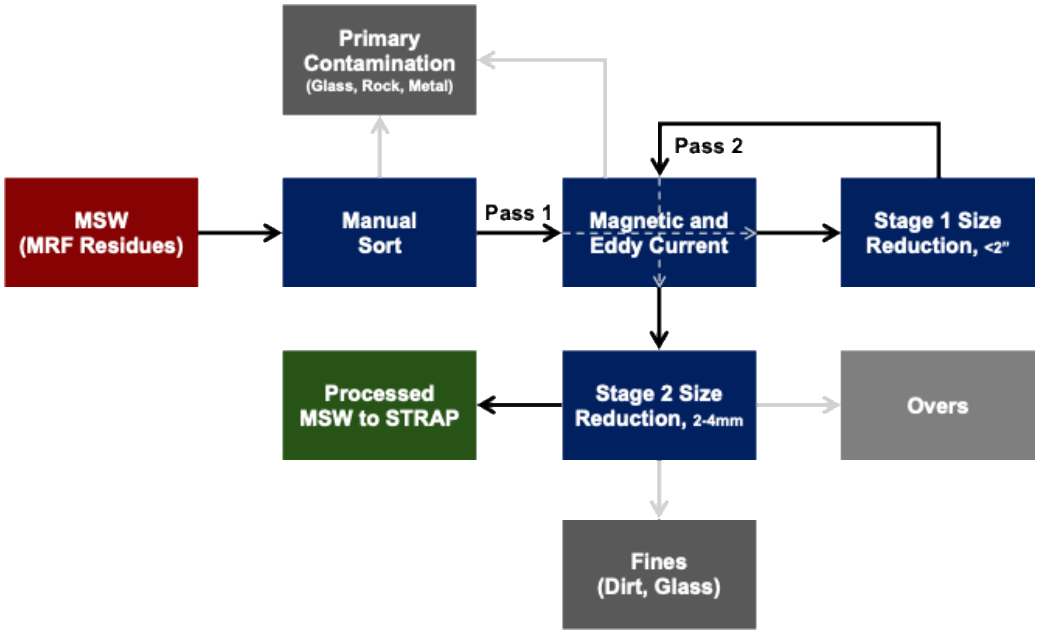

Supplementary Fig. 15. Pre-processing flow diagram.

Two MSW feedstocks were used in this study: one sourced from a MRF in Salt Lake City, Utah (Waste Management, wm.com) and the other from a similar facility in Ann Arbor, Michigan (Recycle Ann Arbor, recycleannarbor.org). These samples, denoted as MSW-UT and MSW-MI, respectively, specifically refer to the MRF residues, i.e. the fractions remaining after the standard MRF pre-processing operations. To clearly distinguish stages of handling, we define the initial, unprocessed MSW streams arriving at the facilities as raw-MSW-UT and raw-MSW-MI. These raw waste streams underwent a series of manual and mechanical separation steps, including hand sorting, eddy current and magnetic separation, and two-step shredding. During this pre-processing, 12.1% (MSW-UT) and 12.0% (MSW-MI) of the incoming raw waste streams were discarded (e.g., contaminants, fines, and non-conforming rejects), while 87.9% and 88.0% were processed and forwarded as MRF residues used in this study. A pre-processing block flow diagram is shown in Supplementary Fig. 15, where primary contaminations (e.g., unknown liquids, hazardous and biohazardous items, etc.), large metal objects (designated for recycling), and fines were rejected from pre-processing steps and considered for landfilling. Note that overs (larger than the in-spec size) may also be classified as reject streams in this process; however, these streams can be recycled back into the size-reduction step in a continuous operation facility.

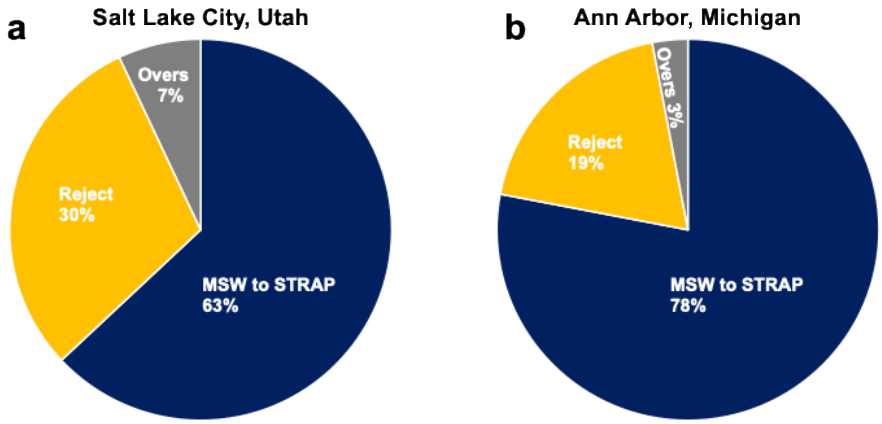

Supplementary Fig. 16. Mass balance of MSW preprocessing.
a, MSW from Salt Lake City, Utah, and **b,** MSW from Ann Arbor, Michigan.

Briefly, the raw MSW went through manual sorting to remove large non-convertible objects (e.g., glass, rocks, and metals) along with biological hazards (e.g., medical waste and diapers), followed by eddy current separation to remove non-ferrous metals, such as aluminum cans. The eddy current operates by inducing repulsive forces through rapidly rotating magnetic fields, which causes conductive materials to be ejected from the main flow. The sorted fraction subsequently underwent the first stage size reduction (< 2 inches) using a VAZ 1100 XL VacoPlan shredder (Greensboro, NC), followed by magnetic separation to remove ferrous metals such as iron and steel using permanent magnets. Finally, a second shredding step using an M24M-30e Series 2 Forest Concept Crumbler (Auburn, WA) was employed to further reduce the size to approximately 2-4 mm, yielding the final MRF residues that were used in the STRAP process. Supplementary Fig. 16 shows the overall mass balance of both MSW feedstocks. Material hold-up inside the pilot scale equipment resulting from the batch size reduction was excluded from mass balance calculations, as such losses are negligible in a continuous processing facility. Pictures of as-received (from the MRFs) and pre-processed MSW feedstocks are shown in Supplementary Fig. 17.

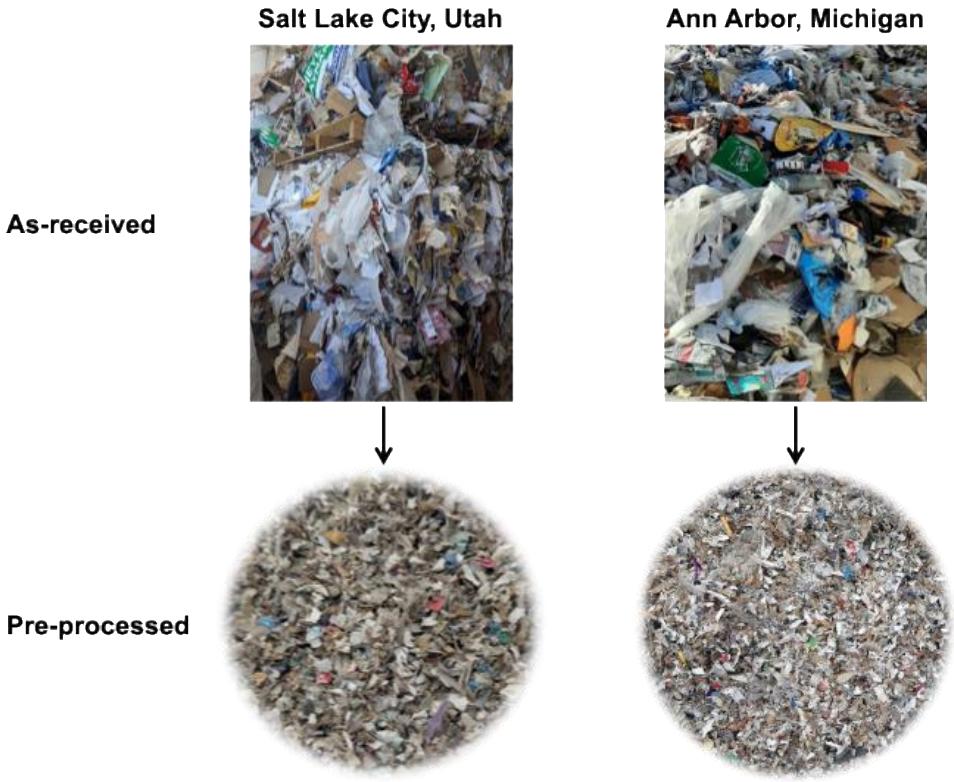

Supplementary Fig. 17. Pictures of as-received and pre-processed MSW from Salt Lake City, Utah and Ann Arbor, Michigan.

These MRF residues (MSW-UT and MSW-MI), enriched in mixed plastics and biogenic material, were used as the feedstocks for all downstream processes, including STRAP extraction, enzymatic hydrolysis, and fermentation. No chemical pretreatments were applied prior to STRAP processing to preserve the heterogeneity of the samples and maintain process relevance to realistic mixed waste management scenarios.

The virgin polymer resins used in this study were LDPE (DOW 608A), HDPE (Sigma-Aldrich 427985), PP (Sigma-Aldrich 427888). The solvents in this study were xylene (technical grade, mixture of isomer, Aqua Solutions), toluene (ACS reagent, ≥99.5 %, Sigma-Aldrich), and GVL (ReagentPlus, 99 %, Sigma-Aldrich).

Supplementary Method 2. Computational Solubility Predictions.

Polymer solubilities in various solvents were computationally predicted using the conductor-like screening model for realistic solvents (COSMO-RS) following the approach developed in our previous work.[17,18] As shown in Supplementary Fig. 1, COSMO-RS represents each solvent or polymer molecule based on a screening charge density that is obtained from density functional theory (DFT) calculations. We approximated the screening charge densities of

polymer molecules by modeling oligomer structures with deactivated terminal groups using conformers obtained from molecular dynamics simulations performed in prior work[17,18] and performing a single-point DFT calculation in the infinite dielectric constant limit using *Gaussian 16* at the BVP86/TZVP/DGA1 level of theory. Screening charge densities for solvents were obtained from our prior work.[17,18] COSMO-RS solubility calculations were performed using COSMOtherm 19 with the BP_TZVP_19 parameterization. Solubilities were computed using solid-liquid equilibrium calculations with resin-specific experimental solubilities obtained from past work used as input to calibrate free energies of fusion estimates in the COSMOtherm calculations.[17,18]

Supplementary Method 3. STRAP Experiment and Evaluation.

Lab-scale STRAP experiments were conducted by loading 15-40 g of MSW into an aramid filter bag (4-inch diameter, 8-inch height, 1 μm pore size). The filter bag was first placed into a 1000 mL beaker, and the selected solvent (xylene, toluene, or GVL) was then added to fully cover the MSW. The beaker was heated in an oil bath to the target temperature. Once it reached the target temperature, the mixture was maintained at the temperature for 1 hour. The filter bag was immediately removed from the beaker after 1 h of dissolution, allowing the solvent to fully drain back into the beaker. Afterward, the beaker was cooled to induce polymer precipitation, and the precipitated polymer was recovered by filtration and dried in a vacuum oven at 100 °C. Comparable extraction results were also obtained using a modified Soxhlet setup, which allowed processing of larger MSW quantities under similar solvent and thermal conditions.

Scale-up STRAP experiments were conducted using a jacketed dissolution vessel equipped with an internal 100 μm pore size metal filter bucket. An aramid filter bag (7-inch diameter and 16.5-inch height, 1 μm pore size) was placed inside the bucket to prevent the release of fine biogenic materials and dust present in MSW into the solvent during dissolution. Approximately 200 g of MSW was loaded into the aramid filter bag and an organic solvent (e.g. xylene) was added in a sufficient amount (~6 L) to fully submerge the MSW. The vessel jacket was connected to an external thermal oil pump that heated and circulated silicone oil, maintaining the reaction temperature (130 °C for xylene). The experiment was held at this temperature for 3 hours to enable polymer dissolution, and after the reaction, the solvent was immediately drained from the vessel. Then, the solvent was cooled to allow polymer precipitation, and the resulting solids were collected via filtration, followed by drying in a vacuum oven at 100 °C.

To evaluate STRAP performance, the initial masses of the MSW, filter bag, and filter paper were measured prior to each experiment. After the process, the recovered polymer (collected on the filter paper) and the biogenic residue (retained in the filter bag) were dried in a vacuum oven at 100 ℃ and weighed. The mass of the recovered polymer was determined by subtracting the pre-measured weight of the empty filter paper from the total dried mass of the filter paper with polymer. The polymer yield (wt%) was calculated as the ratio of the recovered polymer mass to the initial MSW mass. The mass of the biogenic residue was obtained by subtracting the weight of the empty filter bag from the dried weight of the filter bag containing the residue. The overall mass balance (wt%) was then calculated by summing the masses of the recovered polymer and the biogenic residue and dividing by the initial MSW mass.

Supplementary Method 4. Enzyme Hydrolysis & Fermentation Experiments and Evaluation

Biogenic MSW was hydrolyzed at three different scales (2 g, 10 g, 100 g) using Cellic CTec 2 enzyme (Novozymes) at ~7.5% w/w enzyme loading in 10 mM sodium acetate buffer (pH 5.0). Kanamycin (50 $\mu g \cdot mL^{-1}$) or autoclaving was used to inhibit microbial contamination. Reactions were incubated at 52 ℃, 230 rpm for 72 h. Hydrolysates were clarified by centrifugation (16,128 × g, 20 min) and sequential filtration (0.45 μm PVDF and 0.22 μm nylon), then stored at -20 ℃ after pH adjustment to 5.8. To assess microbial contamination, hydrolysates were plated on LB and PDA agar with chloramphenicol and incubated at 37 ℃ for 7 days. Isolated colonies were identified via 16S/26S rRNA gene amplification and Sanger sequencing.

Fermentations were performed using engineered *Saccharomyces cerevisiae* strain GLBRCY1348.[19,20] Cultures were grown to mid-log phase in YPD medium, harvested, washed, and inoculated into MSW hydrolysates (OD600 = 0.2). Cultures were incubated anaerobically at 30 ℃, 150 rpm for 48 h and monitored using a respirometer system. Fermentation supernatants were analyzed by HPLC for metabolites and sugar conversion.

Metabolite concentrations were quantified by HPLC-RID (Aminex HPX-87H column) under isocratic elution with 0.02 N H_2SO_4 at 50 ℃. Glucose, xylose, ethanol, glycerol, and organic acids were quantified using external calibration curves. Statistical significance was determined by two-sample t-tests ($p < 0.05$).

Eq. 1. Titer = $[product]_T - [product]_{CTec}$

where $[product]_T$ is the concentration of product in CTec-treated MSW sample.

Eq. 2. Yield from MSW = $100 \times titer \times V_{hydrolysate} / m_{MSW}$

where $V_{hydrolysate}$ is the volume of recovered liquid hydrolysate, and m_{MSW} is the mass of MSW in the hydrolysis sample.

Eq. 3.

$N_{product} = titer \times V_{hydrolysate} / M_{product}$

where $N_{product}$ is the moles of product yielded from hydrolysis, $V_{hydrolysate}$ is the volume of recovered liquid hydrolysate, and $M_{product}$ is the molecular weight of the product (180.16 $g \cdot mol^{-1}$ for glucose and 150.13 $g \cdot mol^{-1}$ for xylose).

$T_{product} = m_{MSW} \times f_{product} / M_{product}$

where $T_{product}$ is the total moles of product in the MSW sample, m_{MSW} is the mass of MSW in the hydrolysis sample, and $f_{product}$ is the mass fraction of MSW composed of product as determined by compositional analysis.

Glucose saccharification yield = $100 \times N_{glucose} / T_{glucose}$

Xylose saccharification yield = $100 \times N_{xylose} / T_{xylose}$

Fermentable sugars saccharification yield = $100 \times (N_{glucose} + N_{xylose}) / (T_{glucose} + T_{xylose})$

Eq. 4. Fermentation rate = $titer_{ethanol} / time_{CO2,max}$

where $titer_{ethanol}$ is ethanol titer and $time_{CO2,max}$ is the time at which CO_2 concentration reaches its maximum or remains unchanged for one hour, whichever is sooner.

Eq. 5. Ethanol theoretical process yield from fermentation = $100 \times [ethanol]_{final} / (([glucose]_{initial} + [xylose]_{inital}) / 0.511)$

where $[ethanol]_{final}$ is the concentration of ethanol post-fermentation, $[glucose]_{initial}$ is the concentration of glucose pre-fermentation, and $[xylose]_{inital}$ is the concentration of xylose pre-fermentation.

Eq. 6. Ethanol theoretical process yield from fermentation = $100 \times [ethanol]_{final} / (([glucose]_{initial} + [xylose]_{inital} + (2 \times [cellobiose]_{inital}))/ 0.511)$

where $[cellobiose]_{inital}$ is the concentration of cellobiose pre-fermentation.

Eq. 7. Ethanol yield from MSW = $100 \times titer_{ethanol} \times V_{hydrolysate} / m_{MSW}$
where $titer_{ethanol}$ is ethanol titer, $V_{hydrolysate}$ is the volume of recovered liquid hydrolysate, and m_{MSW} is the mass of MSW in the hydrolysis sample.

Eq. 8. Ethanol theoretical process yield from hydrolysis and fermentation = $100 \times titer_{ethanol} \times V_{hydrolysate} / 46.068 / (T_{glucose} + T_{xylose}) / 2$
where $titer_{ethanol}$ is ethanol titer, $V_{hydrolysate}$ is the volume of recovered liquid hydrolysate, $T_{glucose}$ is the total moles of glucose in the MSW sample, and T_{xylose} is the total moles of xylose in the MSW sample.

Supplementary Method 5. Characterization

Thermogravimetric analysis (TGA) was performed on a TGA 500 and a TGA 5500 (TA Instruments) analyzer for 10-20 mg of the recovered polymer by heating them to 800 °C with a rate of 20 °C min^{-1} under nitrogen atmosphere. TGA isotherm analysis was conducted with the isotherm temperature at 190 °C for 30 min.

Attenuated total reflectance Fourier-transform infrared (ATR-FTIR) spectra were acquired using a Bruker Vertex 70 FTIR spectrometer (Bruker). A total of 16 scans were recorded in the spectral range of 4000-600 cm^{-1} at a resolution of 4 cm^{-1}, with air serving as the background reference.

Thermal characterization of polymer was conducted using a DSC 214 Polyma (NETZSCH) and a Q100 (TA) under a nitrogen atmosphere (80 mL·min^{-1}). Approximately 10 mg of sample was sealed in aluminum pans with lids. The thermal program began with equilibration at 40 °C for 5 min, followed by heating to 200 °C at a rate of 10 °C·min^{-1}, an isothermal hold for 5 min, cooling to 40 °C at 10 °C·min^{-1}, 5 min isothermal hold, and a second heating to 200 °C at the same rate. Melting temperature (T_m) and crystallization temperature (T_c) were determined from the resulting thermograms.

Elemental composition of the samples was determined using a vario EL cube elemental analyzer (Elementar). The instrument allows simultaneous quantification of carbon (C), hydrogen (H), nitrogen (N), and sulfur (S) with high sensitivity and precision. Approximately 5 mg of sample was weighed into tin capsules and combusted in an oxygen-rich atmosphere at high temperature. The gases were detected using a thermal conductivity detector (TCD). The instrument was calibrated using certified standards, and blank measurements were included to

ensure accuracy. Each sample was tested in 10 replicates, and the mean value was used for reporting.

For ash content analysis, crucibles were first pre-treated by heating at 575 ℃ to remove any residual moisture or organics. After cooling, they were stored under vacuum in a desiccator until use to ensure accurate baseline mass. Approximately 3 g of each sample was weighed into the pre-treated crucibles and combusted at 575 ℃ for 3 h in a muffle furnace. The residual ash was weighed after cooling. Ash content was calculated as a weight percentage of the initial sample mass. Each sample was analyzed in 5 replicates, and the average value was reported.

The melt flow index (MFI) of the samples was measured using an extrusion plastometer (Tinius Olsen M987) following ASTM D1238. Tests were conducted at 190 ℃ under a 2.16 kg load. Each sample was tested in 5 replicates, and the average value was reported. For the tensile test, extruded pellets were subsequently injection molded into ASTM D638 Type I specimens. Then, tensile testing was performed according to ASTM D638 at a crosshead speed of 5 $mm \cdot min^{-1}$. Rheological measurements on molded discs (25 mm Ø × 2 mm) were obtained via frequency sweeps at 0.1% strain and 190 ℃ to determine complex viscosity across a broad (0.01 – 100 Hz) frequency range on a Bohlin CVO100 rheometer.

For composition analysis of 2 g MSW hydrolysis samples, moisture and ash contents were determined according to ASTM D1102 and D1108, respectively. Fixed carbon content was measured at 950 ℃ per ASTM E870. Soxhlet extraction with CH_2Cl_2 was performed to quantify extractives, and lignin content (Klason and acid-soluble) was determined using a modified ASTM D1106 protocol. Extractive-free samples were hydrolyzed with 72% H_2SO_4 at 30 ℃ for 1 h, followed by dilution and autoclaving (121 ℃, 30 min). Acid-soluble lignin was quantified at 205 nm ($\varepsilon = 110\ L \cdot g^{-1} \cdot cm^{-1}$), and monosaccharides were analyzed by HPLC using dual Rezex RPM columns with RI detection, following ASTM E1758.

For 10-100 g hydrolysis experiments, compositional analysis was conducted using NREL LAP protocols. Extractives were obtained by sequential water and ethanol extraction using an accelerated solvent extractor. Water-soluble sugars were released by acid hydrolysis (4% H_2SO_4), autoclaved at 121 ℃ for 1 h, neutralized, filtered (0.2 μm), and analyzed by HPLC (Aminex HPX-87P, RI detection). Acid-insoluble and acid-soluble lignin were quantified via gravimetry and UV-Vis spectroscopy (240 nm, $\varepsilon = 25$). Organic acids were determined using an Aminex HPX-87H column and diode array detection. Ash content was measured by combustion at 575 ℃ and reported on a 105 ℃ dry basis.

Supplementary Method 6. Life Cycle Assessment (LCA)

The goal of the LCA is to determine the potential environmental benefits of the STRAP-MSW waste-valorization process against the conventional production routes for ethanol, polymer resins, and electricity. The system boundary extends from cradle to biorefinery-gate for the operational phase and does not include the construction phase of the biorefinery. All operational data in the life cycle inventory originated from the biorefinery model leveraged in this study (Supplementary Table 26 and Section 3). Environmental impacts associated to the consumption of each raw material and ancillary input were adapted from the GREET 2023 model and the ecoinvent 3.7 life cycle inventory database.[21,22] The life cycle impact assessment methodology used was the Intergovernmental Panel on Climate Change (IPCC) 2013,[23] with a focus on GWP_{100} (reported herein as carbon intensity) as the primary indicator driving government incentives. The fossil fuel consumption and water consumption were also evaluated and discussed (detailed results presented in Supplementary Sections 3 and 5). The material balance closure around water is listed in Supplementary Table 29. A key assumption used in this study is that all associated environmental impacts (including emissions, fossil fuel consumption, and water usage) of the MRF residues waste are zero. This is a standard assumption for consumer waste products such as MSW which would be generated, collected, and transported to a landfilling or processing facility regardless.[24–26]

We employed energy-based allocation to estimate the carbon intensities of ethanol, electricity, and energy-dense plastic resin products (Supplementary Section 3). The allocation factors and environmental impacts of each product and representative scenario combination are listed in Supplementary Tables 27-28. Other allocation methods were considered less suitable. Mass-based allocation was not pursued because it cannot be applied to electricity coproducts.[27] Economic allocation addresses alternative product end uses by allocating environmental impacts based on the market revenue of each product. Due to the high variability in product prices, the International Organization for Standardization's guideline 14044 suggests that economic allocation should not be considered when methods based on physical properties are available.[28] The Renewable Fuel Standard mandate, as employed by the United States Environment Protection Agency (U.S. EPA), favors the displacement allocation method (i.e., system expansion),[29] whereby coproducts displace the impacts of market products outside the system boundary. However, the plastic resin product has unclear end uses (e.g., as a component in recycled plastic or a feed to pyrolysis upgrading) and all products are produced in similar amounts (on an energy basis), making it difficult to justify a single main product.

Among all alternative routes, corn stover ethanol has the lowest carbon intensity per unit energy, making the carbon intensity of corn stover ethanol the most conservative benchmark to compare against. For this reason, we focus our discussion on detailed comparisons between STRAP-MSW ethanol production against corn stover ethanol using a functional unit of 1 L of ethanol. However, detailed LCA results of electricity, polymer resin, and ethanol are detailed in Supplementary Section 3.

Supplementary Method 7. Techno-Economic Analysis (TEA)

Cost estimates for the solvent removal equipment were provided by Amcor. Cost estimates for specialized STRAP equipment (e.g., dissolution and precipitation vessels) were provided by industry vendors. The 6/10th rule for economies of scale was used to formulate capital cost correlations for the specialized modules in STRAP.[30] The costs of the adsorption columns were estimated as pressure vessels using ASME guidelines to vessel thickness.[31] The cost correlations of specialized ethanol production equipment (e.g., bioreactors, pressure filter) and for utility systems (e.g., co-heat and power generation, cooling tower, chilled water generation) were adapted from NREL's cellulosic ethanol biorefinery model.[32] All other equipment cost correlations originate from various public sources,[30,33] as detailed by Cortés-Peña et al.[34] The chemical engineering plant cost index (used to account for the increasing cost of equipment due to inflation) was assumed to be 816. All parameters used in the discounted cash flow analysis follow the assumptions made in NREL's cellulosic ethanol report,[32] except for the baseline federal corporate tax, which was updated to 21%. Because all simulated scenarios were found to achieve over 60% reduction in carbon intensity relative to a 2016 petroleum benchmark established by the U.S. Environmental Protection Agency (U.S. EPA)[35] (see the Results and Discussion section), the techno-economic analyses included the value of the renewable identification numbers (RINs) of cellulosic biofuel (i.e., D3 RIN) pathway following the guidance of 75 FR 14863.[36] RIN credits were treated as a co-product and decreased the minimum selling price (MSP) of the plastic resin. The MSP was calculated assuming an internal rate of return (IRR) of 10%. A breakdown of the estimated revenue and capital and operating expenditures can be found in Supplementary Section 1 and 5.

Supplementary Method 8. Uncertainty and Sensitivity

The STRAP-MSW process is an early-stage technology and subject to uncertainty in key inputs, including processing capacity (MRF-residue availability), tipping fees, solvent

separation performance, and ethanol conversion efficiency. To quantify how these uncertainties propagate to economic and environmental outcomes, we performed Monte Carlo uncertainty analysis and global sensitivity analysis . Two key scenario subspaces were considered: the "baseline subspace" (assuming the demonstrated experimental performances for ethanol hydrolysis and fermentation; Supplementary Section 1) and the "potential subspace" (assuming the theoretical upper limit for the performance of ethanol production technology; Supplementary Section 1). In both subspaces, STRAP-MSW facility was assumed to be sited close to Boston, Massachusetts, with a tipping fee of 113.0 USD·MT^{-1} and a processing capacity of 30,000 MT·yr^{-1}.[37–39] The "full problem space", which considers all uncertainties and future theoretical improvements, was used to conduct the global sensitivity analysis and the full results are detailed in Supplementary Section 5.

A total of 23 economic and technological performance parameters were varied in Monte Carlo simulations (Supplementary Section 3). Fuel and electricity prices were updated to include the latest market prices from the U.S. Department of Agriculture (USDA) Economic Research Service (ERS),[40] the U.S. Energy Information Administration,[41] and the U.S. EPA.[42] Latin hypercube sampling was used to generate 10,000 scenarios which were used to evaluate the full problem space. A total of 10,000 scenarios were also sampled at each scenario subspace representing key alternative assumptions on ethanol production performance, MSW tipping fee, and MSW processing capacity. Halving the number of scenarios resulted in no significant change in uncertainty and sensitivity results. The sensitivity of the MSP and carbon intensity to each input parameter was characterized by Spearman's rank-order correlation, a measure of monotonicity between input and output parameters. In contrast to single-point sensitivity analyses, which make a baseline assumption and disregard nonlinear interactions between input parameters, Spearman's correlation coefficient provides a more rigorous measure of sensitivity across the full landscape of potential outcomes. Monte Carlo simulations across the processing capacity were performed for 500 points at 12 processing capacities (500 × 12; 6,000 scenarios evaluated) for each scenario subspace. Parameters not explicitly varied were set to the baseline values (Supplementary Section 2-3). A Gaussian filter was applied to smooth discontinuities originating from automated discrete design decisions (e.g., number of fermenters in parallel).

Supplementary Method 9. Techno-Economic and Environmental Assessment Framework

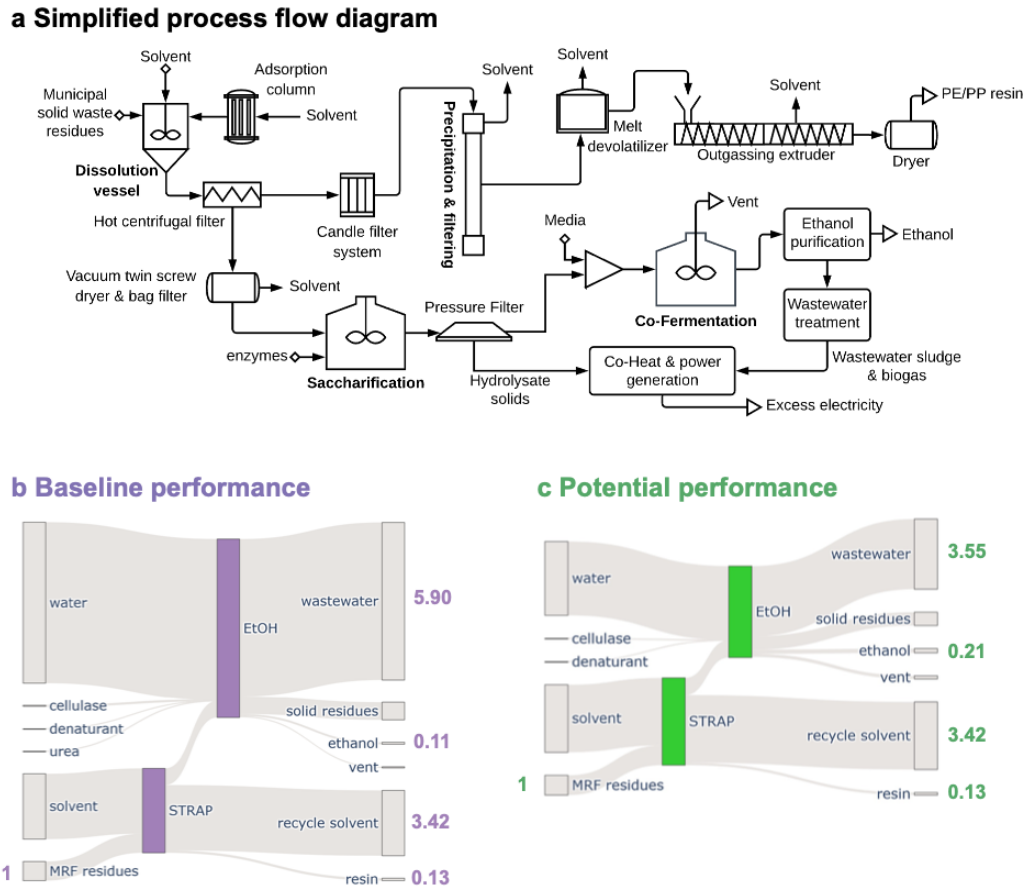

Supplementary Fig. 18. a, Simplified process flow diagram of STRAP-MSW detailing the STRAP, hydrolysis, and fermentation operations. Auxiliary unit operations, including pumps, storage tanks, and heat exchangers are omitted for clarity. **b-c,** Sankey diagrams of the mass flow rate through the STRAP and ethanol processing areas for the baseline scenario (**b**) and the potential scenario (**c**) for improved ethanol production performance, not including wastewater treatment, heat and power generation, and other facilities. The labeled numbers represent the relative flow rate with respect to the MRF residues. The baseline scenario operates at low fermentation titers (~11.5 $g \cdot L^{-1}$) compared to the potential scenario (~54.0 $g \cdot L^{-1}$), leading to a larger recirculation of water at the baseline scenario.

The conceptual STRAP-MSW biorefinery design builds upon prior TEA/LCA frameworks for STRAP and cellulosic ethanol production.[43–47] Post-MRF residues containing mixed plastics and biogenic material are contacted with xylene in a dissolution vessel to selectively dissolve PE/PP (Supplementary Fig. 18). The slurry is separated via centrifugal filtration and the dissolved resin is recovered by cooling-induced precipitation in a jacketed precipitation/filtration module. Solvent is removed from the precipitated resin using conventional plastics-processing equipment (e.g., melt devolatilization followed by outgassing extrusion) to reduce solvent content from ~80 wt% to <1 wt% and ultimately to <10 ppm in

the final resin. To manage the buildup of soluble contaminants (e.g., additives, inks, and soluble biogenic components) in the circulating solvent, a granulated activated carbon adsorption step was included based on established design procedures (Supplementary Section 1-5).

The undissolved solids from STRAP are vacuum dried and routed directly to enzymatic hydrolysis and fermentation for ethanol production. Process design and costing of the ethanol production section was adapted from Cortés-Peña et al., excluding biomass pretreatment and hydrolysate concentration.[45] Wastewater from ethanol purification is treated using a multistage anaerobic process suitable for cellulosic biorefinery effluents which have high organic loading rates.[46] Because hydrolysis and fermentation of MSW-derived biogenic residues remain early-stage technologies, we evaluated two scenarios: a baseline case reflecting experimentally demonstrated ethanol performance (titer ~11.5 $g \cdot L^{-1}$) and a potential case reflecting improved performance consistent with NREL cellulosic ethanol targets (titer ~54 $g \cdot L^{-1}$). Achieving these improvements depends on optimizing hydrolysis and fermentation conditions (e.g., enzyme loading and hydrolysate solids loading) for post-STRAP residues, whose composition and physical characteristics may vary across MSW streams. Under baseline assumptions, solvent recirculation and wastewater generation were 3.42× and 5.90× the MRF-residue feed rate, respectively (Supplementary Fig. 18b). Under the potential case, wastewater generation substantially decreased (3.55× the feed rate; Supplementary Fig. 18c).

Supplementary Section 1-5: STRAP-MSW TEA and LCA.

Process Design and Simulation

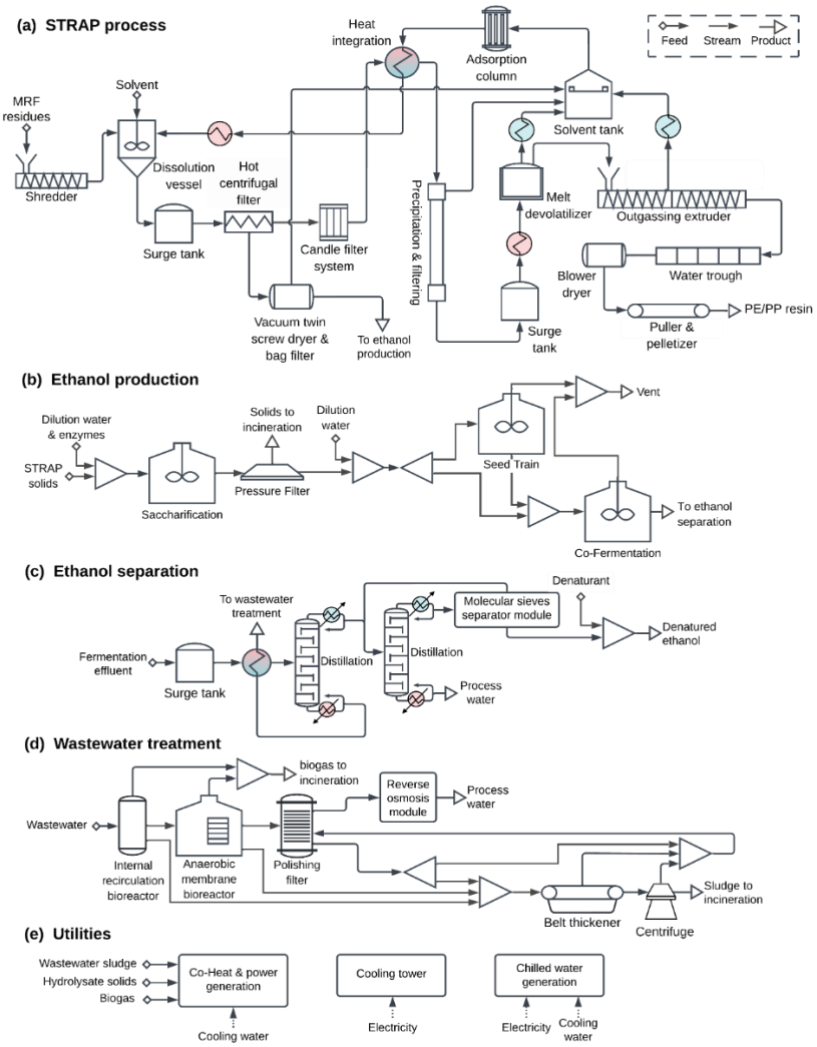

Supplementary Fig. 19. Simplified process flow diagram of the STRAP-MSW process, including (**a**) STRAP process, (**b**) ethanol production, (**c**) ethanol separation, (**d**) wastewater treatment, and (**e**) utility production systems (e.g., boiler and turbogenerator, cooling tower). Pumps and storage are omitted for clarity.

The conceptual STRAP-MSW biorefinery design builds upon past TEA/LCA studies on STRAP and cellulosic ethanol production.[43–47] The feedstock is composed of the remaining biogenic material and plastic after preprocessing MSW at a MRF. The feedstock is fed to a dissolution vessel and is mixed with xylene solvent to dissolve PE/PP (Supplementary Fig. 19a). The effluent is sent to a centrifugal filter to separate the solids (i.e., insoluble plastics and biogenic material) from the solution. The dissolved resin is then precipitated by cooling within a jacketed precipitation and filtration module. The precipitated product has a solvent content

of 80% while the wet insoluble solids stream has a solvent content of 50%, based on experimental observations. In previous studies, convective drying (by air) and extrusion was assumed, which leads to unrecovered solvent. In this study, key improvements were made to the STRAP configuration to maximize solvent recovery from these streams. Firstly, we implemented a vacuum twin-screw drier to recover 99.99% of the solvent retained on the solid product of the centrifugal filter. On the backend after precipitation, we employed the same technology used in the plastic industry to remove solvents from the product resin, including a melt devolatilizer, which melts resin with a high solvent content (~80 wt%) and vaporizes the solvent down to < 1 wt%, and an outgassing extruder to achieve low concentrations of < 10 ppm in the resin. Plastic additives, inks, and any soluble biogenic material which may accumulate in the solvent are removed by adsorption with granulated activated carbon. The design of the adsorption module follows the procedure outlined by Gabelman.[48] The solute capacity was estimated using the fitted Freundlich isotherm of Yellow 12 dye (commonly found in plastics) with activated carbon.[49] The length of unused bed was estimated through numerical mass transfer modeling. After adsorption, the cold solvent must then be reheated and sent back to the dissolution tank. To improve the energy efficiency and overall economics, a heat exchanger was introduced between the hot and cold solvent streams. This also makes the process less sensitive to low precipitation temperatures and high dissolution and boiling point temperatures.

The solids stream from the STRAP process is fed to the ethanol production section (Supplementary Fig. 19b). The design and costing of the ethanol production process (i.e., saccharification, fermentation, and ethanol separation) follows the design configuration outlined by Cortés-Peña et al., excluding the biomass pretreatment and the hydrolysate concentration.[45] In contrast to the highly cited biorefinery model developed at NREL which removes the solids after fermentation, we opted to separate the solids before the fermentation.[47] Introducing deadweight solids in the fermentation bioreactor, which include lignin, unhydrolyzed cellulose and hemicellulose, and insoluble plastic not extracted in the STRAP process, would lead to increased capital (e.g., more fermentation vessels) and operational expenses (e.g., agitation power, maintenance of impellers). Detailed assumptions on the saccharification and fermentation operation and performance are detailed in Supplementary Section 1. The separation of ethanol uses a conventional configuration with design specifications in agreement with previous studies on cellulosic ethanol production (Supplementary Fig. 19c).[45,47] The bottom product from the beer column is sent to a multistage

anaerobic wastewater treatment process designed for treating wastewaters with high organic loading rates distinctive to cellulosic biorefinery wastewaters (Supplementary Fig. 19d).[46]

Supplementary Section 1. Input Parameter Distributions and Baseline Values

A total of 21 economic, environmental, and technological performance parameters were varied in Monte Carlo simulations (Supplementary Table 20). Assumptions for the full problem space are outlined in Supplementary Table 20. Assumptions for scenario analyses, whereby certain assumptions are constrained to reduce the dimensionality of the system, are detailed in Supplementary Table 21. Normal distributions were truncated at ±2σ to prevent outliers. Baseline assumptions on feedstock composition are detailed in Supplementary Table 22.

Supplementary Table 20. Input parameter assumptions and distributions for the full problem space.

#	Parameter	Units	Baseline	Distribution	Ref
1	MRF residue tipping fee	USD·MT^{-1}	113	Normal(μ=64.5, σ=39.4)	37–39
2	Residue biogenic content	wt%	78.1	Uniform(73.1, 83.1)	c
3	Plastics solute content	wt%	0.005	Uniform(0.001, 0.01)	a
4	Residue processing capacity	10^3·MT·yr^{-1}	30	Uniform(30, 133)	b, 37
5	Solvent (xylene) price	USD·kg^{-1}	2.17	Uniform(1.63, 2.71)	50
6	Extracted polymer mass fraction	wt% plastic	16.8	Uniform(15.1, 18.5)	a
7	Centrifuged plastic solvent content	%	50	Uniform(40, 60)	a
8	Precipitate solvent content	%	80	Uniform(70, 90)	a
9	Extracted polymer to solvent ratio	wt%	5	Uniform(2, 10)	a
10	Ethanol price	USD·L^{-1}	0.358	Triangular(0.272, 0.272, 0.548)	40
11	RIN D3 price	USD·RIN^{-1}	0.534	Triangular(0.349, 0.553, 0.701)	42
12	Electricity price	cents·kWh^{-1}	6.89	Triangular(6.67, 6.83, 7.18)	41
13	Cellulase price	USD·kg^{-1}	0.212	Uniform(0.159, 0.265)	32
14	Cellulase loading	wt% cellulose	2.668	Uniform(2.668, 0.667)	a, 32
15	Saccharification solids loading	wt% solids	9.52	Uniform(9.52, 20)	a, 32
16	Cellulase GWP	kgCO2e·kg^{-1}	8.05	Uniform(7.25, 8.86)	21
17	Saccharification glucose yield	%	44.7	Uniform(28.5, 90)	a, 32

18	Saccharification xylose yield	%	38.1	Uniform(38.1, 90)	a, 32
19	Cofermenation sugar to ethanol yield	%	74.7	Uniform(73.4, 91.4)	a, 32
20	Cofermentation ethanol productivity	$g \cdot L^{-1} \cdot h^{-1}$	0.468	Uniform(0.458, 1.5)	a, 32
21	Cofermentation ethanol titer	$g \cdot L^{-1}$	11.5	Uniform(11.3, 54)	a, 32
22	Operating days	day	330	Constant	a
23	IRR	%	10	Constant	a
24	MSW GWP	$kgCO2e \cdot kg^{-1}$	0	Constant	

[a] This study.
[b] The processing capacity for the baseline scenario is equivalent to the processing capacity of Casella Waste System Inc in Boston, MA. The upper bound assumes that a MRF can be constructed to process 770,000 MT of MSW annually (equivalent to a large-sized landfill) and 19% of MSW is residue that would feed into a STRAP-MSW facility.
[c] The uncertainty in the biogenic content, which depends on the sitting of the STRAP-MSW facility and the time of the year, has not been quantified yet. It is assumed to be ±5 wt%.
[d] The actual cellulase loading used in the hydrolysis experiments was an excess amount that would result in an ethanol production cost equivalent to 10× the price of ethanol. To ensure that the uncertainty analysis is industry relevant, we assume that a cellulase loading of 4× the amount assumed by NREL is sufficient to attain similar hydrolysis conversions.

Supplementary Table 21. Constrained parameter assumptions and distributions for key ethanol production scenarios.

Parameter	**Units**	**Baseline[a]**	**Potential[b]**
Saccharification glucose yield	%	44.7	90
Saccharification xylose yield	%	65.8	90
Cofermenation sugar to ethanol yield	%	Normal(μ=74.7, σ=1.3)	91.4
Cofermentation ethanol productivity	$g \cdot L^{-1} \cdot h^{-1}$	Normal(μ=0.468, σ=0.1)	1.5
Cofermentation ethanol titer	$g \cdot L^{-1}$	Normal(μ=11.5, σ=0.2)	54

[a] Values were based on experimental results from this study.
[b] Values were based on the set of assumptions listed for NREL's cellulosic ethanol production model, which is assumed to be the maximally attainable performance for MSW biogenic material with future advancements.[5] All other parameters (e.g., tipping fee, processing capacity) are set to the baseline values.

Ethanol prices were fitted over 5 years (May 2017–May 2022) of historical prices from the U.S. Department of Agriculture (USDA) Economic Research Service (ERS).[40] Prices for cellulosic biofuel (D3) Renewable Identification Numbers (RINs) were also fitted over the same period.[42] The range of years was limited to 5 because of limited availability of recorded D3 RIN prices (e.g., no recorded price before 2013). The price of electricity was fitted over 5 years of historical prices (2017–2022) from the U.S. Energy Information Administration.[41] The mean of each price distribution is used to create the baseline scenario for detailed TEA results. The number of operating days for processing MSW was assumed to be 330 days. The internal rate of return (IRR) was assumed to be 10%, which is recommended for waste-reducing

biorefineries.[51] The characterization factor for the cellulase cocktail was modeled as uniform distributions with lower and upper limits equal to ±10% of the baseline values obtained from the GREET 2022 model.

Supplementary Table 22. Baseline composition of feedstock based on compositional analysis from this study.

	MRF residue composition (%)
PEPP	16.8
Insoluble plastic	5.13
Inks and xylene solubles	0.005
Ash	8.74
Lignin	26.8
Extractives	3.29
Soluble lignin	1.87
Glucan	32
Xylan	5.29

Supplementary Section 2. Capital and Operating Costs

All techno-economic calculations and the cash flow analysis were made following the procedure outlined by Humbird et. al.[32] for the production of cellulosic ethanol from corn stover. Material prices of feeds come from various sources, including text books and literature.[30,32,50] The chemical engineering plant cost index (CEPCI) used in this study was 816. Supplementary Tables 23-25 list capital and operating expenditures under the baseline set of assumptions and the potential attainable fermentation performance with future research and development. Supplementary Fig. 20 shows the heating and cooling duties for both scenarios.

Supplementary Table 23. Capital expenditures for the STRAP-MSW process under representative assumptions.

	Notes	baseline (MM$)	potential (MM$)
ISBL installed equipment cost		32.2	28.1
OSBL installed equipment cost		25.2	22.6
Warehouse	4.0% of ISBL	1.29	1.12
Site development	9.0% of ISBL	2.89	2.53
Additional piping	4.5% of ISBL	1.45	1.26
Total direct cost (TDC)		63	55.6
Proratable costs	10.0% of TDC	6.3	5.56
Field expenses	10.0% of TDC	6.3	5.56
Construction	20.0% of TDC	12.6	11.1
Contingency	40.0% of TDC	25.2	22.3
Other indirect costs (start-up, permits, etc.)	10.0% of TDC	6.3	5.56
Total indirect cost		56.7	50.1
Fixed capital investment (FCI)	TDC + TIC	120	106
Working capital	5.0% of FCI	5.98	5.29
Total capital investment (TCI)	FCI + WC	126	111

Supplementary Table 24. Variable operating costs and product sales for the STRAP-MSW process under representative assumptions.

		Price ($·MT^{-1})	baseline (MM$·yr^{-1})	potential (MM$·yr^{-1})
Raw materials	**FGD lime**	199	0.00747	0.00241
	MSW	-113	-3.37	-3.37
	NaOCl	140	0.000203	0.0000866
	Xylene	2170	0.0111	0.0111
	Activated carbon	3.06	0.0000936	0.0000936
	Bisulfite	79.9	0.0000185	0.00000788
	Boiler chemicals	5000	0.00141	0.00109
	Cellulase	1590	2.7	0.676
	Citric acid	337	0.000205	0.0000873
	Cooling tower chemicals	3000	0.00137	0.000775
	Denaturant	756	0.0529	0.104
	Urea	99.2	0.0122	0.00501
Other utilities & fees	**Ash disposal**	31.8	0.013	0.0129
	Process water	0.27	0.00125	0.000838
Co-products & credits	**Electricity production**	454	1.48	2.89
	Ethanol	0.06895 $/kWh	1.49	1.57
	Ethanol RIN D3	677	0.262	0.514
Variable operating cost (including co-products & credits)			-0.834	-1.74
Products	**Resin**	1510	13.5	5.81

Supplementary Table 25. Fixed operating costs for the STAP-MSW process under representative assumptions.

	Notes	baseline (MM$·yr^{-1})	potential (MM$·yr^{-1})
Labor salary	-	0.6	0.6
Labor burden	90% of labor salary	0.54	0.54
Maintenance	3.0% of ISBL	0.964943	0.842767
Property insurance	0.7% of FCI	0.837597	0.740068
Fixed operating cost (FOC)		2.942539	2.722836

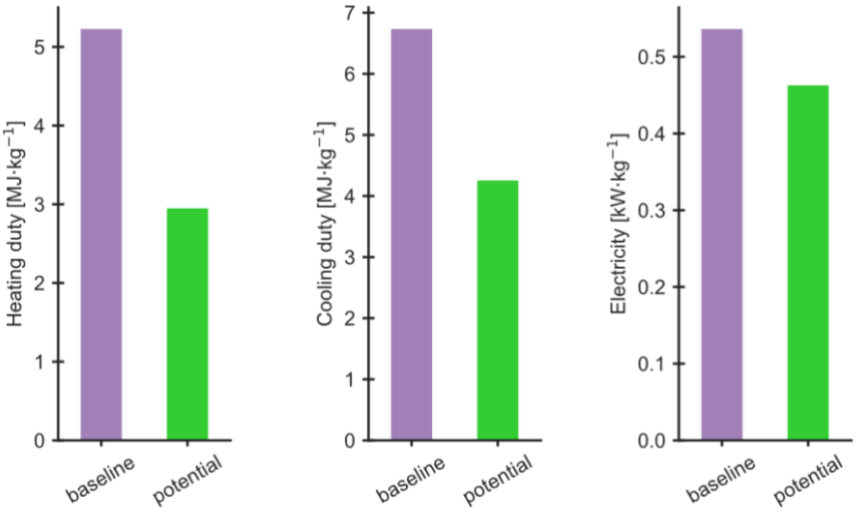

Supplementary Fig. 20. Bar plot of the cooling duty, heating duty, and electricity consumption for the STRAP-MSW production process at the baseline and potential scenarios.

Supplementary Section 3. Life Cycle Assessment Across Allocation Methods

The cradle-to-gate life cycle carbon intensity (measured as 100-year global warming potential, GWP_{100}), fossil fuel consumption, and water usage was quantified by energy allocation. The life cycle inventory, allocation factors, and environmental impacts of ethanol for each of the representative scenario are listed in Supplementary Tables 26-28. The material balance around water is listed in Supplementary Table 29.

Supplementary Table 26. Life cycle inventory.

		Baseline inventory [kg·yr^{-1}]	Potential inventory [kg·yr^{-1}]
Inputs	**Lime**	37500	12100
	NaOCl	1460	620
	Xylene	5110	5110
	Bioreactor cleaning chemicals	31500	31500
	Bisulfite	232	98.7
	Boiler makeup water	4370000	3380000
	Cellulase	1700000	425000
	Citric acid	609	259
	Cooling tower makeup water	19900000	11300000
	Denaturant	70000	137000
	Makeup process water	38900000	26100000
	Saccharification water	2.48E+08	1.04E+08
	Stripping water	3570000	7720000
	Urea	123000	50500
Outputs	**Polymer resin**	3850000	3850000
	RO treated water	24200000	14600000
	Ethanol	3250000	6380000
	Recycled process water	2.52E+08	1.12E+08
	Electricity [kWhr·yr^{-1}]	21500000	22800000
Direct non-biogenic emissions		409	409

Supplementary Table 27. Energy allocation factors.

	Baseline energy allocation factors	Potential energy allocation factors
Electricity	0.283	0.226
Ethanol	0.396	0.531
Polymer resin	0.321	0.243

Supplementary Table 28. Estimated well-to-gate carbon intensity (GWP_{100}), fossil fuel consumption (FFC), and water usage (WU) of products.

		Baseline	Potential
Electricity	**GWP [kg·CO_2e·kWh^{-1}]**	0.0298	0.00689
	FFC [MJ·kWh-^{1}]	0.175	0.0405
	WU [L_{H2O}·kWh^{-1}]	0.189	0.0438
Ethanol	**GWP [kg·CO_2e·L^{-1}]**	0.201	0.106
	FFC [MJ·L^{-1}]	1.18	0.626
	WU [L_{H2O}·L^{-1}]	1.28	0.676
Polymer resin	**GWP [kg·CO_2e·kg^{-1}]**	1.28	0.572
	FFC [MJ·kg^{-1}]	7.52	3.37
	WU [L_{H2O}·kg^{-1}]	8.12	3.64

Supplementary Table 29. Water mass balance, including all process water inputs, treated RO-grade water outputs (from wastewater treatment), water losses to emissions and brine, and reactions consumption/producing water.

		Water [kg·hr^{-1}]
Feeds	**Cellulase**	42.9
	Saccharification water	12400
	Stripping water	918
	NaOCl	0.0645
	Bisulfite	0.00728
	Cooling tower makeup water	1340
	Cooling tower chemicals	0.0307
	Bioreactor cleaning chemicals	3.74
	Boiler makeup water	402
	Flue gas desulfurization lime	0.708
Treated/recycled	**RO treated water**	11900
Losses	**Ethanol (trace water in product)**	4.97
	Brine	157
	Cooling tower blowdown	122
	Cooling tower evaporation	1220
	Bioreactor cleaning wastewater	3.74
	Emissions	2063.4
	Boiler blowdown water	402
Reacted	**Saccharification U201**	137
	Internal circulation reactor U301	36.6
	Anaerobic MBR U302	4.98
	Polishing filter U303	-2.04
	Boiler turbogenerator BT401	-1000
Mass balance error (Feeds - Recycled - Losses - Reacted)		0

Supplementary Section 4. Detailed Techno-Economic and Life Cycle Assessment Insights

The economic performance and environmental impacts of the baseline and potential scenarios were evaluated using TEA and LCA (Supplementary Fig. 21 and Section 2). Under the baseline and potential ethanol-performance scenarios, the total revenue was 1.9× and 3.6× higher than operating costs, respectively (Supplementary Fig. 21b). The sources of revenue driving this high profit margin are the sales of resin, ethanol, and electricity, and the credits for the residue tipping fee and RIN D3 (cellulosic biofuel credits under the U.S. Renewable Fuel Standard). The operating costs were dominated by fixed costs (e.g., labor, maintenance, insurance) and cellulase enzyme procurement. Despite the favorable profit margin, high capital expenditures led to long payback periods of 22 years (baseline) and 11 years (potential). The capital costs were dominated by indirect costs (e.g., construction and contingency; 40% of direct costs) and by site facilities and utilities (e.g., wastewater treatment and heat/power generation systems), reflecting the substantial heating, cooling, and power demands of the STRAP-MSW process.

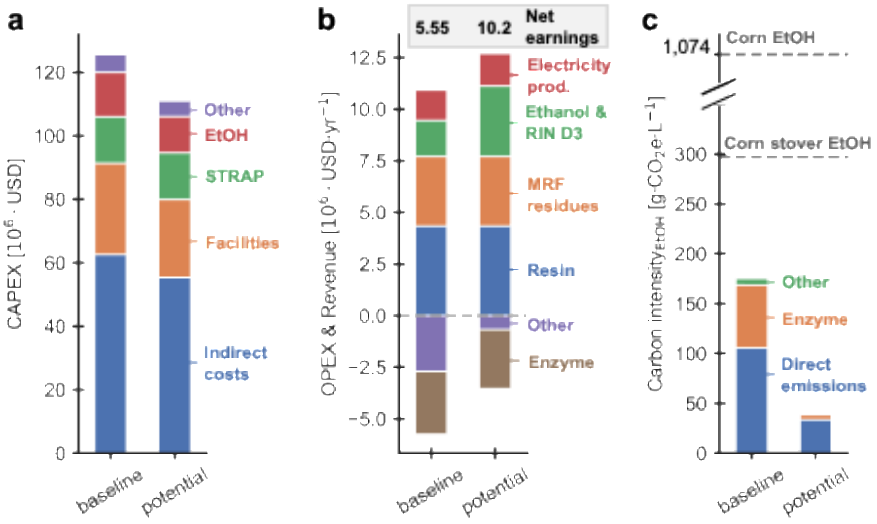

Fig. 21. TEA/LCA results for a 30 kton MSW/year plant (a-c) including: (a) capital expenditures, (b) operating costs, credits, and revenue, and (c) carbon intensity of ethanol. In panel (a): "facilities" (in orange) include wastewater treatment and utility modules (e.g., boiler, turbogenerator, cooling tower), and "other" (in purple) include other direct costs (i.e., warehouse, site development, additional pipping). In panel (b): variable operating costs such as nutrients for fermentation and chemicals for wastewater treatment are negligible and are not included in the plot.

Ethanol production from MRF residues remains an emerging technology with substantial room for improvement. Relative to the baseline scenario, the potential scenario reduces capital costs by 13% (primarily from ethanol production and facilities), lowers enzyme costs by 75%,

increases revenue from ethanol and RIN credits by 2.5×, and decreases ethanol carbon intensity by 74%. Achieving these gains depends on optimizing enzyme loading and hydrolysate solids loading for post-STRAP residues, whose composition and physical characteristics vary across MSW streams; data-driven models that link residue features to optimal hydrolysis conditions and pretreatment method could improve transferability across sites.

Supplementary Section 5. Monte Carlo Simulations and Sensitivity Analysis

Monte Carlo uncertainty analysis was performed for the full problem space listed in Supplementary Table 20 as well as for the baseline and potential fermentation performance subspaces listed in Supplementary Table 21 (Supplementary Fig. 22 and 23). The sensitivity of the MSP and carbon intensity to each input parameter was characterized by Spearman's rank-order correlation, a measure of monotonicity between input and output parameters (Supplementary Fig. 24-25).

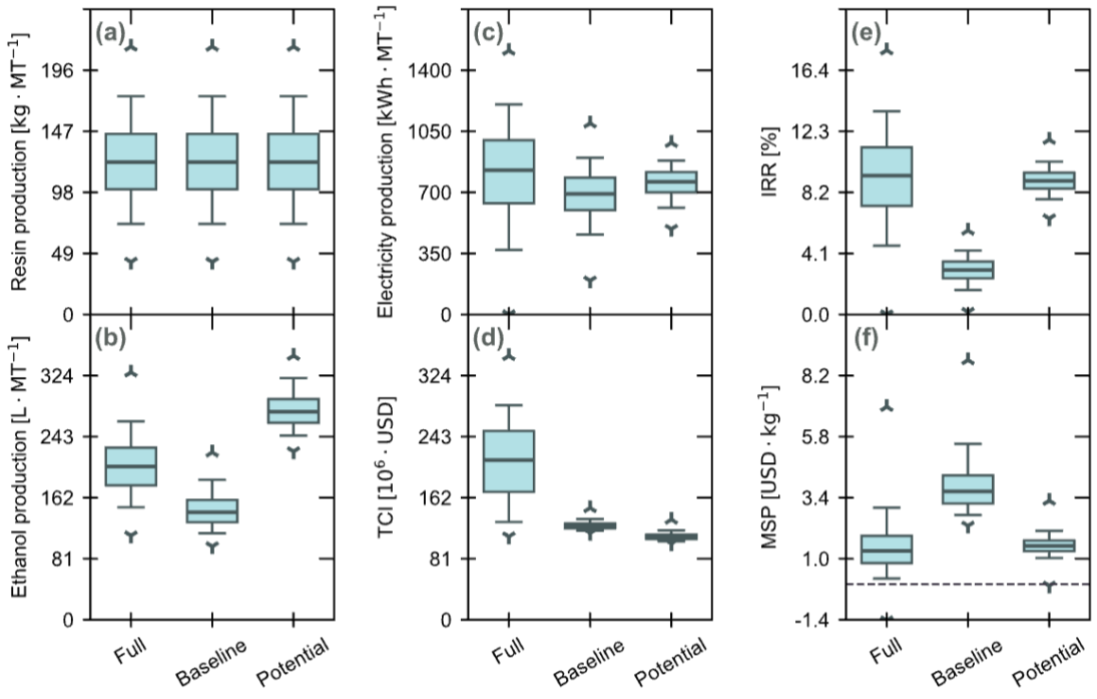

Supplementary Fig. 22. Box and whiskers plot of the Monte Carlo techno-economic analysis results for the full problem space, the subspace with baseline assumptions on fermentation performance, and the subspace with potential assumptions on an improved fermentation performance. Results are presented with median values (dark, solid lines), 25th to 75th percentiles (shaded region), and 5th and 95th percentiles (whiskers).

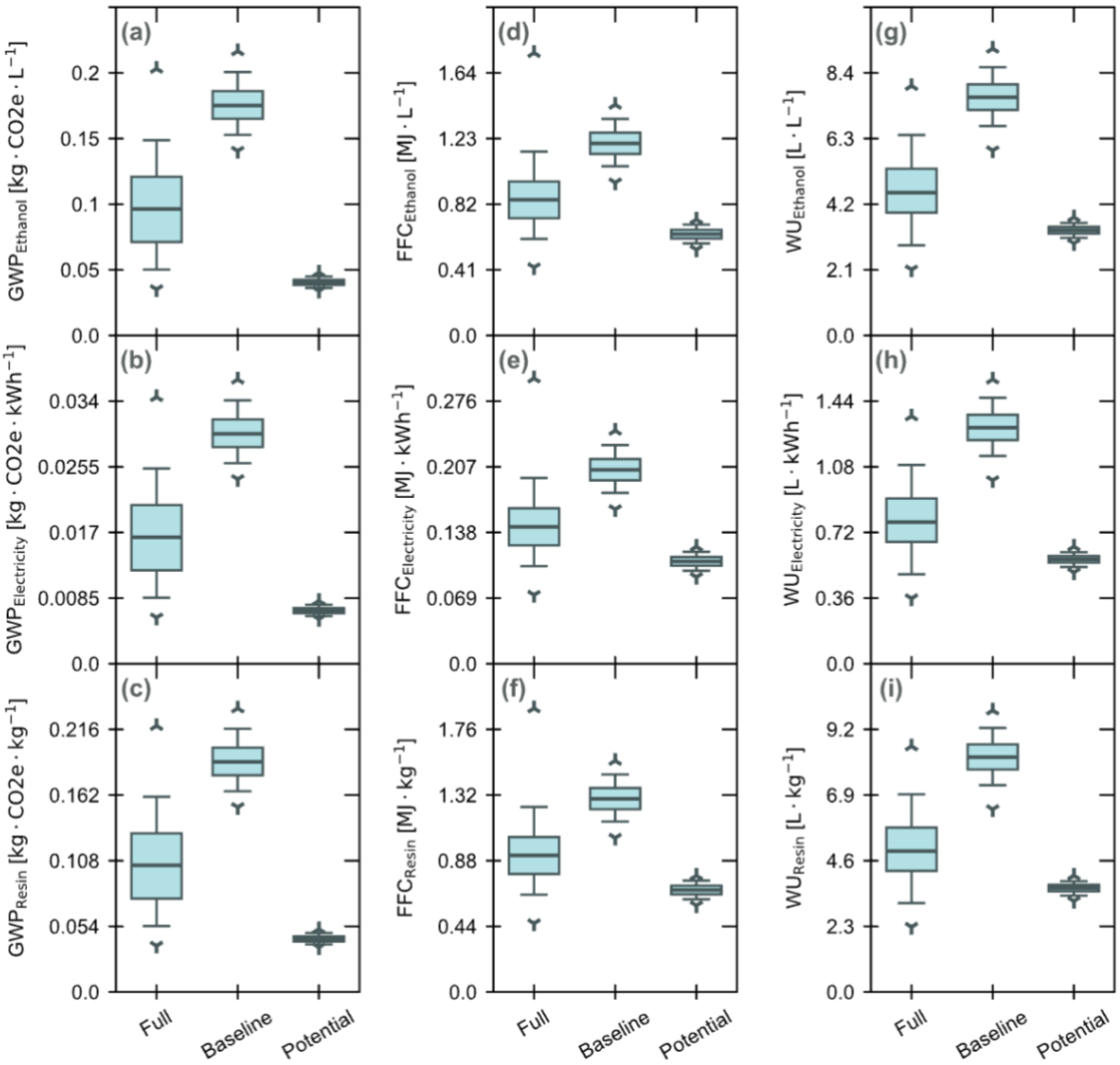

Supplementary Fig. 23. Box and whiskers plot of the Monte Carlo life cycle assessment results for the full problem space, the subspace with baseline assumptions on fermentation performance, and the subspace with potential assumptions on an improved fermentation performance. Results are presented with median values (dark, solid lines), 25th to 75th percentiles (shaded region), and 5th and 95th percentiles (whiskers).

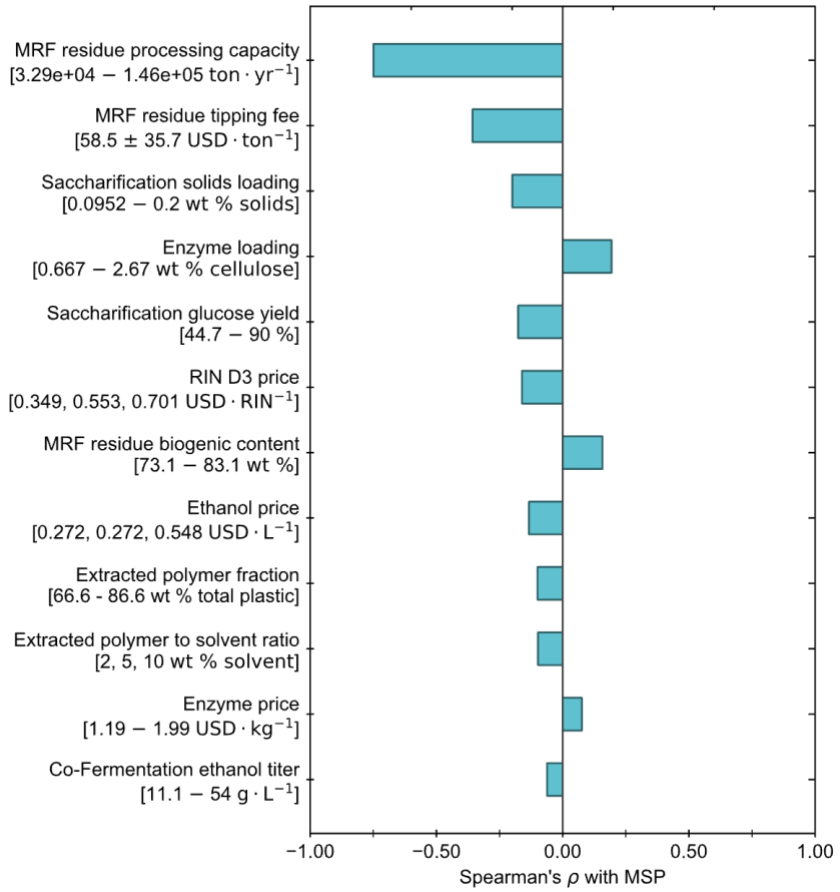

Supplementary Fig. 24. Sensitivity of the MSP to parameters varied in the Monte Carlo simulations, as determined by Spearman's rank correlation coefficients (ρ). Only parameters with |ρ| > 0.02 are shown. The values in brackets represent the distributions of each parameter. Parameters with triangular distributions list the minimum, most probable, and maximum values in brackets. Parameters with uniform distributions list the minimum and maximum values in brackets. Parameters with normal distributions list the mean followed by the standard deviation.

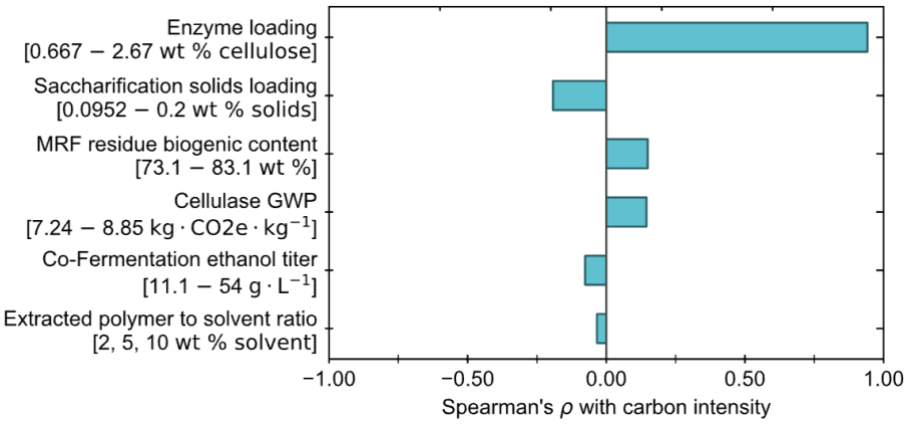

Supplementary Fig. 25. Sensitivity of the carbon intensity to parameters varied in the Monte Carlo simulations, as determined by Spearman's rank correlation coefficients (ρ). Only parameters with |ρ| > 0.02 are shown. The values in brackets represent the distributions of each parameter. Parameters with triangular distributions list the

minimum, most probable, and maximum values in brackets. Parameters with uniform distributions list the minimum and maximum values in brackets.

References

1. Zaikova, A., Falsafi, A., Falsafi, A., Abdulkareem, M. & Horttanainen, M. Transition to recycling versus incineration in municipal solid waste management: Evaluating the speed of greenhouse gas emission reduction. *Waste Manag. Res.* **43**, 2104–2115 (2025).
2. Enache, M.-M., Gavrilescu, D. & Teodosiu, C. Comparative Analysis of Plastic Waste Management Options Sustainability Profiles. *Polymers* **17**, (2025).
3. Abedin, T. *et al.* From waste to worth: advances in energy recovery technologies for solid waste management. *Clean Technol. Environ. Policy* **27**, 5963–5989 (2025).
4. Soni, A., Gupta, S. K., Rajamohan, N. & Yusuf, M. Waste-to-energy technologies: a sustainable pathway for resource recovery and materials management. *Mater. Adv.* **6**, 4598–4622 (2025).
5. Ragaert, K., Delva, L. & Van Geem, K. Mechanical and chemical recycling of solid plastic waste. *Waste Manag.* **69**, 24–58 (2017).
6. Tamizhdurai, P. *et al.* A state-of-the-art review of multilayer packaging recycling: Challenges, alternatives, and outlook. *J. Clean. Prod.* **447**, 141403 (2024).
7. Jiang, J. *et al.* From plastic waste to wealth using chemical recycling: A review. *J. Environ. Chem. Eng.* **10**, 106867 (2022).
8. Oliveux, G., Dandy, L. O. & Leeke, G. A. Degradation of a model epoxy resin by solvolysis routes. *Polym. Degrad. Stab.* **118**, 96–103 (2015).
9. Clark, R. A. & Shaver, M. P. Depolymerization within a Circular Plastics System. *Chem. Rev.* **124**, 2617–2650 (2024).
10. Shah, H. H. *et al.* A review on gasification and pyrolysis of waste plastics. *Front. Chem.* **10**, (2023).
11. Zhang, J. *et al.* Powering air travel with jet fuel derived from municipal solid waste. *Nat. Sustain.* **8**, 1480–1490 (2025).

12. Kaushal, R., Rohit & Dhaka, A. K. A comprehensive review of the application of plasma gasification technology in circumventing the medical waste in a post-COVID-19 scenario. *Biomass Convers. Biorefinery* **14**, 1427–1442 (2024).
13. Nagar, V. & Kaushal, R. A review of recent advancement in plasma gasification: A promising solution for waste management and energy production. *Int. J. Hydrog. Energy* **77**, 405–419 (2024).
14. Fei, F., Wen, Z., Huang, S. & De Clercq, D. Mechanical biological treatment of municipal solid waste: Energy efficiency, environmental impact and economic feasibility analysis. *J. Clean. Prod.* **178**, 731–739 (2018).
15. Peti, D., Dobránsky, J. & Michalík, P. Recent Advances in Polymer Recycling: A Review of Chemical and Biological Processes for Sustainable Solutions. *Polymers* **17**, (2025).
16. Schade, A. *et al.* Plastic Waste Recycling─A Chemical Recycling Perspective. *ACS Sustain. Chem. Eng.* **12**, 12270–12288 (2024).
17. Zhou, P., Yu, J., Sánchez-Rivera, K. L., Huber, G. W. & Lehn, R. C. V. Large-scale computational polymer solubility predictions and applications to dissolution-based plastic recycling. *Green Chem.* **25**, 4402–4414 (2023).
18. Zhou, P., Sánchez-Rivera, K. L., Huber, G. W. & Van Lehn, R. C. Computational Approach for Rapidly Predicting Temperature-Dependent Polymer Solubilities Using Molecular-Scale Models. *ChemSusChem* **14**, 4307–4316 (2021).
19. Chandrasekar, M. *et al.* A high solids field-to-fuel research pipeline to identify interactions between feedstocks and biofuel production. *Biotechnol. Biofuels* **14**, 179 (2021).
20. Lee, S.-B. *et al.* Crabtree/Warburg-like aerobic xylose fermentation by engineered *Saccharomyces cerevisiae*. *Metab. Eng.* **68**, 119–130 (2021).
21. Michael Wang *et al. Summary of Expansions and Updates in GREET® 2020*. (2020).

22. Wernet, G. *et al.* The ecoinvent database version 3 (part I): overview and methodology. *Int. J. Life Cycle Assess.* **21**, 1218–1230 (2016).
23. T.F. Stocker *et al. IPCC, Climate Change 2013: The Physical Science Basis*. https://www.ipcc.ch/report/ar5/wg1/.
24. Dominguez Aldama, D., Grassauer, F., Zhu, Y., Ardestani-Jaafari, A. & Pelletier, N. Allocation methods in life cycle assessments (LCAs) of agri-food co-products and food waste valorization systems: Systematic review and recommendations. *J. Clean. Prod.* **421**, 138488 (2023).
25. Wang, J. *et al.* Life cycle assessment of the integration of anaerobic digestion and pyrolysis for treatment of municipal solid waste. *Bioresour. Technol.* **338**, 125486 (2021).
26. Islam, Md. M., Haque, N., Lau, D., Bhuiyan, M. & Pramanik, B. K. Comparative life cycle assessment of end−of−life strategies for post−consumer polylactic acid waste: Environmental trade−offs and uncertainty analysis. *Chem. Eng. J.* **522**, 167057 (2025).
27. Sandin, G., Røyne, F., Berlin, J., Peters, G. M. & Svanström, M. Allocation in LCAs of biorefinery products: implications for results and decision-making. *J. Clean. Prod.* **93**, 213–221 (2015).
28. International Organization for Standardization. *ISO 14044:2006 Environmental Management — Life Cycle Assessment — Requirements and Guidelines*. (2006).
29. U.S. Environmental Protection Agency. Regulation of Fuels and Fuel Additives: Changes to Renewable Fuel Standard Program; Final Rule. *Fed. Regist.* **75**, 14670–14904 (2010).
30. Seider, W. D. *et al. Cost Accounting and Capital Cost Estimation. In Product and Process Design Principles*. (Wiley, 2017).
31. Seider, W. D., Seader, J. D. & Lewin, D. R. *Product and Process Design Principles: Synthesis, Analysis and Design*. (John Wiley & Sons).

32. D. Humbird *et al. Process Design and Economics for Biochemical Conversion of Lignocellulosic Biomass to Ethanol (Dilute-Acid Pretreatment and Enzymatic Hydrolysis of Corn Stover)*. http://www.nrel.gov/docs/fy11osti/47764.pdf (2011).
33. Don W. Green & Marylee Z. Southard. *Perry's Chemical Engineers' Handbook 9th Edition*. (McGraw-Hill Education: New York, NY, 2018).
34. Cortes-Peña, Y., Kumar, D., Singh, V. & Guest, J. S. BioSTEAM: A Fast and Flexible Platform for the Design, Simulation, and Techno-Economic Analysis of Biorefineries under Uncertainty. *ACS Sustain. Chem. Eng.* **8**, 3302–3310 (2020).
35. US EPA. *Summary Table of Lifecycle Greenhouse Gas Emissions for Select Pathways*. https://www.epa.gov/fuels-registration-reporting-and-compliance-help/summary-table-lifecycle-greenhouse-gas-emissions (2016).
36. Regulation of Fuels and Fuel Additives: Changes to Renewable Fuel Standard Program. *Federal Register* https://www.federalregister.gov/documents/2010/03/26/2010-3851/regulation-of-fuels-and-fuel-additives-changes-to-renewable-fuel-standard-program (2010).
37. Aber, S. 2022 MSW Landfill Tipping Fees | EREF. *Environmental Research & Education Foundation* https://erefdn.org/2022-msw-landfill-tipping-fees/ (2023).
38. Voloschuk, C. On the rebound. *Recycl. Today* https://www.recyclingtoday.com/article/largest-material-recovery-facilities-on-the-rebound/ (2023).
39. Bradshaw, S. L., Aguirre-Villegas, H. A., Boxman, S. E. & Benson, C. H. Material Recovery Facilities (MRFs) in the United States: Operations, revenue, and the impact of scale. *Waste Manag.* **193**, 317–327 (2025).
40. *U.S. Bioenergy Statistics*. https://www.ers.usda.gov/data-products/us-bioenergy-statistics (2022).

41. *Annual Energy Outlook 2021*. https://www.eia.gov/outlooks/aeo/.

42. *RIN Trades and Price Information*. https://www.epa.gov/fuels-registration-reporting-and-compliance-help/rin-trades-and-price-information.

43. Sánchez-Rivera, K. L. *et al.* Reducing Antisolvent Use in the STRAP Process by Enabling a Temperature-Controlled Polymer Dissolution and Precipitation for the Recycling of Multilayer Plastic Films. *ChemSusChem* **14**, 4317–4329 (2021).

44. Yu, J. *et al.* High-purity polypropylene from disposable face masks via solvent-targeted recovery and precipitation. *Green Chem.* **25**, 4723–4734 (2023).

45. Cortés-Peña, Y. R., Kurambhatti, C., Eilts, K., Singh, V. & Guest, J. S. Economic and Environmental Sustainability of Vegetative Oil Extraction Strategies at Integrated Oilcane and Oil-Sorghum Biorefineries. *ACS Sustain. Chem. Eng.* **10**, 13980–13990 (2022).

46. Li, Y. *et al.* Design of a High-Rate Wastewater Treatment Process for Energy and Water Recovery at Biorefineries. *ACS Sustain. Chem. Eng.* **11**, 3861–3872 (2023).

47. A. Dutta *et al. Process Design and Economics for Biochemical Conversion of Lignocellulosic Biomass to Ethanol (Thermochemical Pathway by Indirect Gasification and Mixed Alcohol Synthesis)*. http://www.nrel.gov/docs/fy11osti/47764.pdf (2011).

48. A. Gabelman. *Adsorption Basics: Part 1*. (2017).

49. Yan, T. *et al.* Pigment removal from reverse-printed laminated flexible films by solvent-targeted recovery and precipitation. *Sci. Adv.* **11**, eadt5841 (2025).

50. Chemical Catalysis for Bioenergy Consortium (ChemCatBio). Materials Library.

51. Short, W., Packey, D. J. & Holt, T. *A Manual for the Economic Evaluation of Energy Efficiency and Renewable Energy Technologies*. NREL/TP--462-5173, 35391 http://www.osti.gov/servlets/purl/35391-NqycFd/webviewable/ (1995).